


Article

Changing Relationships between Water Content and Spectral Features in Moso Bamboo Leaves under *Pantana phyllostachysae* Chao Stress

Zhanghua Xu ^{1,2,3,*} , Bin Li ¹, Hui Yu ³, Huafeng Zhang ⁴, Xiaoyu Guo ², Zenglu Li ^{2,5}, Lin Wang ¹, Zhicai Liu ¹, Yifan Li ¹, Anqi He ¹ and Xuying Huang ⁶

- ¹ College of Environment and Safety Engineering, Academy of Geography and Ecological Environment, Fuzhou University, Fuzhou 350108, China
 - ² Fujian Provincial Key Laboratory of Resources and Environment Monitoring & Sustainable Management and Utilisation, Sanming 365004, China
 - ³ Key Laboratory of Spatial Data Mining & Information Sharing, Ministry of Education, The Academy of Digital China, Fuzhou University, Fuzhou 350108, China
 - ⁴ Xiamen Administration Center of Afforestation, Xiamen 361004, China
 - ⁵ SEGi University, Kota Damansara, Petaling Jaya 47810, Malaysia
 - ⁶ International Institute for Earth System Science, Nanjing University, Nanjing 210023, China
- * Correspondence: fzucar@fzu.edu.cn

Abstract: Leaf water content (LWC) is very important in the growth of vegetation. LWC and leaf spectra change when the leaves are under pest stress; exploring the change mechanism between LWC, leaf spectra, and pest stress can lay the foundation for pest detection. In this study, we measured the LWC and leaf spectra of moso bamboo leaves under different damage levels, used the Pearson–Lasso method to screen the features, and established a multiple linear regression (MLR) and random forest regression (RFR) model to estimate the LWC. We analyzed the relationship between LWC and spectral features of moso bamboo leaves under *Pantana phyllostachysae* Chao (PPC) stress and their changes. The results showed that: (1) the LWC showed a decreasing trend as the pest level increased. (2) The spectra changed substantially when the leaves were under pest stress. (3) The number and significance of response features associated with the LWC were diverse under different damage levels. (4) The estimation of LWC under different damage levels differed significantly. LWC, leaf spectra, response features, and the model estimation effect were diverse under different damage levels. The correlation between LWC and features was higher for healthy leaves than for damaged and off-year leaves. The two models were more effective in estimating the LWC of healthy leaves but less effective for damaged and off-year leaves. This study provides theoretical support for the prediction of PPC stress and lays the foundation for remote sensing monitoring.

Keywords: *Pantana phyllostachysae* Chao; changing relationships; water content; spectral features; Pearson–Lasso; moso bamboo



Citation: Xu, Z.; Li, B.; Yu, H.; Zhang, H.; Guo, X.; Li, Z.; Wang, L.; Liu, Z.; Li, Y.; He, A.; et al. Changing Relationships between Water Content and Spectral Features in Moso Bamboo Leaves under *Pantana phyllostachysae* Chao Stress. *Forests* **2023**, *14*, 702. <https://doi.org/10.3390/f14040702>

Academic Editor: Giovanna Battipaglia

Received: 13 January 2023

Revised: 17 March 2023

Accepted: 28 March 2023

Published: 29 March 2023



Copyright: © 2023 by the authors. Licensee MDPI, Basel, Switzerland. This article is an open access article distributed under the terms and conditions of the Creative Commons Attribution (CC BY) license (<https://creativecommons.org/licenses/by/4.0/>).

1. Introduction

Bamboo is one of the most important forest resources that is predominantly distributed in tropical and subtropical regions. Currently, there are three major bamboo regions worldwide, namely, the Asia–Pacific, American, and African bamboo regions. According to the latest Global Forest Resources Assessment, the bamboo forest area in Asia is 24.87×10^6 ha, making it the largest bamboo region worldwide. The main bamboo producers are China, Bangladesh, Bhutan, and India. Among them, China is the country with the most abundant bamboo resources worldwide, with more than 7.01×10^6 ha of bamboo forest. Therefore, China is known as the “Kingdom of Bamboo”. With increasing ecological pressure on forests and scarcity of wood resources in recent years, bamboo is now considered an excellent substitute for traditional wood. On 7 November 2022, the Second Global Bamboo

and Rattan Congress was held in Beijing, where the proposal for “Bamboo as a Substitute for Plastic” was put forward, which reflects the importance of sustainability of bamboo products. With the innovation of bamboo use technology, some high-energy-consumption and high-pollution materials have been replaced by bamboo. China’s bamboo winding composites can replace cement, steel, and plastic. Therefore, bamboo has considerable potential in supporting global green development. Among many bamboo species, moso bamboo is the most important species in China with considerable ecological and economic value because of its rapid growth and high rate of use. However, owing to its asexual reproduction and due to invasive growth, its pure forest rate has been rising. Forests that comprise a single species can severely affect forest biodiversity and lead to frequent pest disturbance events. *Pantana phyllostachysae* Chao (PPC) is one of the most common and destructive pests. According to the national survey data of forestry pests released by the National Forest and Grassland Administration, PPC is a level 3 harmful forestry pest in China, with an annual occurrence area of more than 6.7×10^4 ha. Therefore, the harm caused by PPC has become an important factor threatening the health of bamboo forests as well as restricting the production of high-quality bamboo and sustainable development of the bamboo industry. It is of considerable ecological and economic importance to increase monitoring of this pest. The traditional method mainly used for pest monitoring is manual walking surveys. However, using this method, it is difficult to detect pest presence in a timely and thorough manner. Now, we usually use remote sensing technology to detect forest pests; this has achieved positive results [1–3].

The external morphology and internal biochemical composition of moso bamboo leaves appear substantially changed under PPC stress [4–6]. When leaves have been gnawed by the larvae, the stomata of the leaf cannot be closed, which leads to the loss of water, protein, pigments, inorganic salts, and other leaf biochemical components. Symptoms of water shortage and chlorosis become present in the leaves, which can be directly reflected in the spectral information [7]. Therefore, plant damage can be assessed by inverting plant biochemical components through the spectral information of plants [8,9]. Research on the content of plant biochemical components and pest levels has shown that some biochemical components have a pronounced ability to respond to pest stress [10,11], which is of considerable importance in pest identification and monitoring. However, satellite sensors are prone to certain errors when they acquire images, due to the influence of atmosphere, terrain, and illumination conditions. Therefore, it is difficult to quantitatively study the relationship between biochemical components and pest information. Thus, measured spectra are necessary for investigating the microscopic mechanisms of biochemical components and pest information. They are also important in exploring the change mechanisms in plant biochemical components and leaf spectra when pests are present. The quantitative relationships between them can be clarified, which can lay a foundation for real-time, rapid, and large-area monitoring and early warning of pests using satellite images.

As an important biochemical component, LWC plays a vital role in photosynthesis and transpiration in plants [12]. We can determine crop yield and plant health status by monitoring LWC, and this technique has been widely used in agriculture and forestry. For example, LWC is an important indicator for crop yield estimation and can help detect pests [13,14]. Additionally, LWC is closely related to other biochemical components, such as chlorophyll and nitrogen content [15]. In-depth research is important in the physiological monitoring of plants. Therefore, LWC is important in agricultural and forestry monitoring, and examining this indicator has considerable value in scientific research and production applications. Water in leaves absorbs radiant energy in the near-infrared (NIR) and short-wave infrared (SWIR) regions, forming water absorption peaks at 970, 1200, 1450, and 1950 nm [16–18]. These water absorption characteristics have been used to establish correlations with LWC [19–23]. Studies on LWC and leaf spectra have indicated that continuum removal and spectral derivative processing of the original bands can improve the accuracy of LWC estimation [24,25]. However, indices are more reliable than single bands for LWC estimation [26]. Given that LWC is closely related to NIR and SWIR, many

different vegetation water content diagnostic indices have been proposed based on specific water absorption regions in the NIR and SWIR regions (WI, SRWI, MSI, NDII, GVM, RDI, and DWI). However, most of these indices only involve two or three specific bands and are only suitable for estimating the LWC of fixed plants. Therefore, indices based upon the spectral absorption of different plant leaves, which are suitable for different leaf types, have been proposed [27]. The canopy reflectance model and leaf optical model have been combined, and leaf and canopy parameters have been estimated by using the coupled model. This has increased the range of study of water content from the leaf scale to the canopy scale and resulted in an effective earth–sky interface [28]. Several radiation transfer models are now commonly used, including the PROSPECT, LIBERTY, and SAIL models [20,29].

To date, there has been a strong focus on model optimization and feature selection to improve the estimation effect of LWC. However, the relationships between the changing water content and spectral features of vegetation under pest stress have not yet been examined in detail. To address these gaps in the literature, this study classified moso bamboo leaves with different damage levels and investigated the relationship between them as pest damage stress increases. We have investigated the following questions: (1) how do the LWC and leaf spectra change when the leaves are under different damage levels? (2) How can the features of LWC be examined and models be established? (3) How can changes in spectral features be used to determine the presence of insect pests?

2. Materials and Methods

2.1. Study Area

Shunchang County is located in Fujian Province, China (Figure 1). The area is influenced by the subtropical maritime monsoon and continental climate, with abundant rainfall. Due to its unique climate, the forest cover for Shunchang County has reached approximately 80%. The main tree species are *Eucalyptus grandis*, *Ginkgo biloba*, China fir, Horsetail pine, and moso bamboo. Among them, the spatial area of moso bamboo has reached 4.4×10^4 ha. However, pests cause substantial ecological and economic losses to locals every year. Statistics from the forestry department for 2021 have shown that the PPC is one of the most important leaf-eating pests of bamboo forests in this county. Although the local government has invested considerable human and material resources to control pests each year, there are still many pest disaster areas. Therefore, timely monitoring of pest presence is an effective way of mitigating pests and reducing ecological and economic losses.

2.2. Sample Collection and Damage Level Classification

Our group visited the study area for investigation and sample collection on 20–23 August 2019. The principles of sample collection were: (1) sampling locations were selected at different elevations, and (2) leaves in the canopy were randomly selected. We classified moso bamboo leaves into different damage levels refer to the rules described by LY/T 2011–2012, and took the leaf damage rate as the evaluation criteria. Leaf damage rate refers to the percentage of the leaf area of missing and diseased spots in relation to the total leaf area. Leaf damage rate between 0% and 5% refers to healthy leaves (H), leaf damage rate between 5% and 25% refers to mildly damaged leaves (Mi), leaf damage rate between 25% and 50% refers to moderately damaged leaves (Mo), and leaf damage rate > 50% refers to severely damaged leaves (S). A unique growth habits of moso bamboo is its on- and off-year phenomenon, whereby moso bamboo shoots and grows during its “on” year, and then produces whips and changes leaves in its “off” year. The parameters of its biochemical components are quite different during on and off years. [30]. Therefore, to avoid the effects caused by off-year leaves, they were grouped separately (O). In this study, we selected 50 sampling sites (distribution shown in Figure 1) at different elevations, and 5–6 standard bamboo leaves from each of the upper, middle, and lower part of each sampled bamboo

were acquired from each sampling site. Finally, we collected a total of 382 bamboo leaves; the number of leaves for each level were 78 (H), 67 (Mi), 94 (Mo), 79 (S), and 64 (O).

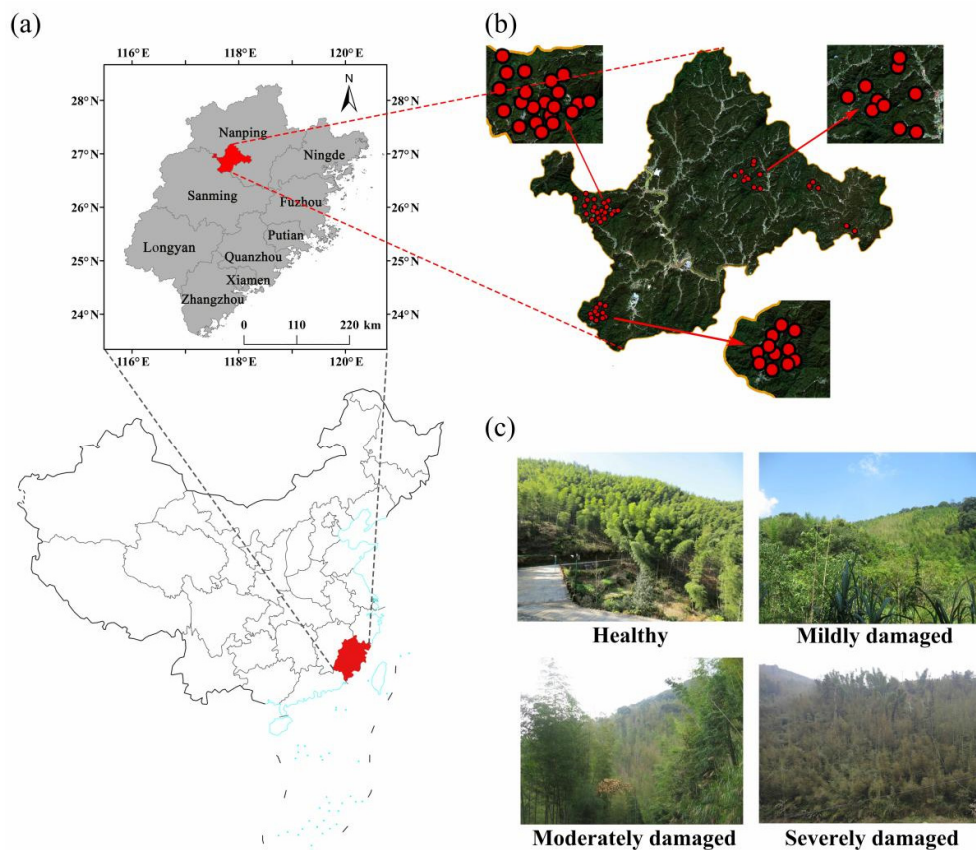


Figure 1. Study area: (a) Shunchang County; (b) sample collection site; (c) moso bamboo with different levels of PPC damage.

2.3. Leaf Physical and Chemical Parameters

2.3.1. Leaf Spectra

An ASD FieldSpec3 spectrometer and an ASD plant spectral probe e (Analytical Spectral devices (ASD) Inc., Longmont, CO, USA) were used for the indoor spectral measurements. The spectral sampling intervals of the spectrometer were 1.4 nm (350–1000 nm) and 2 nm (1001–2500 nm). The resampled bandwidth was 1 nm. The experiment was conducted in a closed environment equipped with a lightbulb to reduce interference from the external environment. The leaves were placed horizontally on a black background, and five frontal spectra were measured and averaged as the leaf spectra. All the spectral data were preprocessed using the Savitzky–Golay smoothing algorithm in Unscrambler X10.4 software to reduce the effects of particle size, scattering, and covariance. The continuum removal method was used to enhance the spectral absorption in the sensitive bands of each biochemical parameter [31].

2.3.2. Leaf Water Content

We collected the moso bamboo leaves from the field site and weighed them at once using a precision electronic scale; the fresh weight was recorded as W_f . The leaves were then brought back to the laboratory and were placed in an oven to kill the enzymes and render them inactive. When the leaves were dried to a constant weight, we weighed the leaves again and the dry weight (W_d) was recorded. The equation for LWC is as follows:

$$LWC = \frac{W_f - W_d}{W_f} \times 100\% \quad (1)$$

where LWC is the leaf water content, W_f is the fresh weight of the leaf, and W_d is the dry weight of the leaf.

2.4. Leaf Spectral Features

2.4.1. Spectral Index

The Spectral index is more reliable than the single band in LWC estimation, and this index is, therefore, widely used for LWC estimation [26]. The absorption capacity of water is different for bands in different regions. In the visible region, the absorption of water by electromagnetic waves is relatively low. Meanwhile, in the NIR and SWIR regions, the absorption is relatively high, and the absorption peak increases with increasing wavelength. Therefore, the indices that are used for LWC estimation are predominantly constructed using bands in the NIR and SWIR regions, including the WI, WBI, and LWI. LWC has a strong correlation with chlorophyll [15]. Some photosynthetic pigment indices and vegetation indices have also been used to estimate LWC, including NDVI, PSSRb, and CI. These indices have had a strong performance in pest stress monitoring and crop water stress monitoring. Mutanga et al. [32] estimated EWT by WI and NDWI and successfully monitored Eurasian wood wasp by observing changes in WI and NDWI. Watt et al. [33] estimated maize leaf water content using NDVI, which provides a theoretical basis for monitoring crop water stress. In this study, we combined previous research results and selected indices related to LWC (Table 1).

Table 1. Indices included in the analysis.

Index	Full Name	Calculation Formula	Source
CI	Chlorophyll index	R_{750}/R_{710}	[34]
GM1	Gitelson and Merzlyak index 1	R_{750}/R_{550}	[35]
GM2	Gitelson and Merzlyak index 2	R_{750}/R_{700}	[35]
MCARI	Modified chlorophyll absorption ratio index	$[(R_{700} - R_{670}) - 0.2(R_{700} - R_{550})](R_{700}/R_{670})$	[36]
PSSRb	Pigment-specific simple ratio chlorophyll b	R_{800}/R_{635}	[37]
TCARI	Transformed chlorophyll absorption ratio index	$3[(R_{700} - R_{670}) - 0.2(R_{700} - R_{550})(R_{700}/R_{670})]$	[38]
TCA/OSAVI	TCARI/OSAVI	TCARI/OSAVI	[38]
VOG	Vogelmann index	R_{740}/R_{720}	[39]
NDVI	Normalized difference vegetation index	$(R_{800} - R_{670})/(R_{800} + R_{670})$	[40]
OSAVI	Optimized soil adjusted vegetation index	$(1 + 0.16)(R_{800} - R_{670})/(R_{800} + R_{670} + 0.16)$	[41]
RDVI	Renormalized difference vegetation index	$(R_{800} - R_{670})/(R_{800} + R_{670})0.5$	[42]
PRI	Photochemical reflectance index	$(R_{531} - R_{570})/(R_{531} + R_{570})$	[43]
Datt ₁	Datt ₁	$(R_{850} - R_{2218})/(R_{850} - R_{1928})$	[17]
Datt ₂	Datt ₂	$(R_{850} - R_{1788})/(R_{850} - R_{1928})$	[17]
DDI	Double difference index	$2R_{1530} - R_{1005} - R_{2005}$	[44]
fWBI	Floating position water band index	$R_{900}/\min(R_{930} - R_{980})$	[45]
GVMi	Global vegetation moisture index	$[(R_{820} + 0.1) - (R_{1600} + 0.02)]/[(R_{820} + 0.1) + (R_{1600} + 0.02)]$	[46]
LWI	Leaf water index	R_{1300}/R_{1450}	[47]
MSI	Moisture stress index	R_{1600}/R_{820}	[48]
MSI ₁	Moisture stress index 1	R_{1650}/R_{1230}	[49]
MSI ₂	Moisture stress index 2	R_{1650}/R_{830}	[49]
NDII	Normalized difference infrared index	$(R_{820} - R_{1600})/(R_{820} + R_{1600})$	[50]
NDWI ₁	Normalized difference water index 1	$(R_{860} - R_{1240})/(R_{860} + R_{1240})$	[51]
NDWI ₂	Normalized difference water index 2	$(R_{870} - R_{1260})/(R_{870} + R_{1260})$	[52]
NDWI ₁₆₄₀	Norm. diff. water index 1640 nm	$(R_{860} - R_{1640})/(R_{860} + R_{1640})$	[53]
NDWI ₂₁₃₀	Norm. diff. water index 2130 nm	$(R_{858} - R_{2130})/(R_{858} + R_{2130})$	[53]
Ratio ₉₇₅	Ratio ₉₇₅	$2\text{mean}(R_{960} - R_{990})/[(\text{mean}(R_{920} - R_{940}) + \text{mean}(R_{1090} - R_{1110}))]$	[34,54]
Ratio ₁₂₀₀	Ratio ₁₂₀₀	$2\text{mean}(R_{1180} - R_{1220})/[(\text{mean}(R_{1090} - R_{1110}) + \text{mean}(R_{1265} - R_{1285}))]$	[34,54]
SIWSI	Shortwave infrared water stress index	$(R_{1640} - R_{858})/(R_{1640} + R_{858})$	[55]
SRWI	Simple ratio water index	R_{860}/R_{1240}	[56]
SRWI ₁	Simple ratio water index 1	R_{1350}/R_{870}	[52]
SRWI ₂	Simple ratio water index 2	R_{880}/R_{1265}	[52]
TM57	Ratio of thematic mapper B5 to B7	R_{1650}/R_{2220}	[57]
WBI	Water band index	R_{970}/R_{900}	[58]
WI	Water index	R_{900}/R_{970}	[59]
SAI ₉₇₀	Spectral absorption index 970	$d = (\lambda_2 - 970)/(\lambda_2 - \lambda_1)$, $\text{SAI}_{970} = (d \times R_1 + (1 - d) \times R_2)/R_{970}$	[27]
SAI ₁₂₀₀	Spectral absorption index 1200	$d = (\lambda_2 - 1200)/(\lambda_2 - \lambda_1)$, $\text{SAI}_{1200} = (d \times R_1 + (1 - d) \times R_2)/R_{1200}$	[27]
SAI ₁₆₀₀	Spectral absorption index 1600	$d = (\lambda_2 - 1600)/(\lambda_2 - \lambda_1)$, $\text{SAI}_{1600} = (d \times R_1 + (1 - d) \times R_2)/R_{1600}$	[27]

Note: λ_1 and λ_2 are the wavelengths corresponding to the wave peaks on the left and right, respectively. R_1 and R_2 are the reflectance of the wave peaks on the left and right, respectively.

2.4.2. Spectral Derivative

The data after the spectral derivative can suppress the background information in the spectra and solve the problem of spectral overlap [60]. They can also amplify subtle changes in the spectral curve, providing a spectral profile with higher resolution and definition than original spectra. Derivative spectra can reflect the change rate of the original spectra and quickly determine the location of the rapid change in the original spectra. This provides the conditions for the selection of water content-sensitive bands. The data after spectral derivation are less affected by the canopy and leaf structure and have advantages in characterizing the total reflectance. Danson et al. [22] treated the spectra with derivative; the result showed that the derivative spectra were insensitive to leaf structure and were closely related to LWC at 1450 nm. Kumar [61] found that derivative spectra have a strong correlation with FMC at the leaf scale. Rollin et al. [25] found that the spectral derivative of grass at 1156 nm was closely related to EWTC. Therefore, in this study, we performed spectral derivative processing on the spectra to improve the response ability between spectra and LWC. The spectral derivative is calculated as follows:

$$R(\lambda_i)' = \frac{R(\lambda_{i+1}) - R(\lambda_i)}{\Delta\lambda} \quad (2)$$

where $R(\lambda_i)$ is the value of reflectance at band i , $R(\lambda_i)'$ is the value of derivative spectra between bands i and $i + 1$, and $\Delta\lambda$ is the step size of neighbor bands.

2.5. Model Feature Screening Method

The Pearson correlation coefficient is often used to measure the linear relationship between variables. We can use this coefficient to screen out features that are more correlated with LWC. However, there may be a problem of collinearity between the features screened by the Pearson correlation coefficient. Stronger collinearity between independent variables may lead to a reduced estimation accuracy of dependent variables [62]. Therefore, effective removal of collinearity between independent variables is an important problem to be addressed. Lasso regression is also known as L1 regularization of linear regression. It uses the regularization term to form a penalty term on the original loss function to prevent the problem of collinearity between independent variables. Therefore, the Pearson–Lasso method was chosen to screen features in this study. We used the Pearson correlation coefficient method to screen features that were related to the LWC first, and then removed the features with strong collinearity using the Lasso regression method for feature selection.

The features used for estimation of the LWC were spectra of continuum removal (SCR), derivative (SD), and the spectral index (SI). Therefore, the features are preliminarily screened using Pearson correlation coefficient, and the calculation formula is [63]:

$$\rho = \text{Cor}(X, Y) = \frac{\text{Cov}(X, Y)}{\sqrt{\text{Var}(X)\text{Var}(Y)}} \quad (3)$$

where $\text{Cov}(X, Y)$ is the covariance of X and Y , and $\text{Var}(X)$ and $\text{Var}(Y)$ are the variances of X and Y , respectively.

2.6. Relationship between LWC and Leaf Spectral Features

To study the relationship between the LWC and spectral features of moso bamboo leaves under PPC stress and their changes over time, we established two models and focused on: (1) how the estimation effect of LWC varies for different damage levels; and (2) how the estimation effect of LWC varies between models. Linear models can reflect simple linear relationships between variables, whereas machine learning can reflect complex nonlinear relationships between variables. We used MLR and RFR to estimate the LWC. We compared the estimation effect of the two models for different damage levels and explored the relationship between the LWC and spectral features of moso bamboo leaves under different damage levels.

MLR is a basic and simple analysis method, that is, a linear regression between one label and multiple features. For sample i with n features, the regression results are as follows:

$$\hat{y}_i = \omega_0 + \omega_1 x_{i1} + \omega_2 x_{i2} + \cdots + \omega_n x_{in} \quad (4)$$

where ω is collectively referred to as the parameter of the model, ω_0 is the intercept, and $\omega_1 \sim \omega_n$ is the regression coefficient.

RFR is a relatively new discriminant model with a decision tree as the unit. It is a bagging integration algorithm that takes the average results of the base evaluator as the result of the integrated evaluator. Therefore, RFR can substantially improve the estimation accuracy. RFR has strong adaptability to datasets, effective anti-noise performance, a strong fitting ability, and it is not easy to produce overfitting with RFR [64].

In this study, we randomly divided the moso bamboo leaf data under different damage levels into a training set (70%) and a test set (30%). A fivefold cross-validation was performed to test model stability. The coefficient of determination (R^2) and root-mean-square error (RMSE) were used to assess the accuracy of the model. The formulas for calculating R^2 and RMSE are as follows:

$$R^2 = 1 - \frac{\sum_{i=1}^n (y_i - \hat{y})^2}{\sum_{i=1}^n (y - \bar{y})^2} \quad (5)$$

$$RMSE = \sqrt{\frac{1}{n} \times \sum_{i=1}^n (y_i - \hat{y})^2} \quad (6)$$

where y is the measured values, \hat{y} is the estimated values, \bar{y} is the mean of all the measured values, and n is the sample size.

2.7. Study Workflow

We mainly divided our work into two parts (Figure 2). In the first part, we collected moso bamboo leaves and then performed preprocessing on them. In the second part, we analyzed the change mechanism of LWC and leaf spectra under different damage levels.

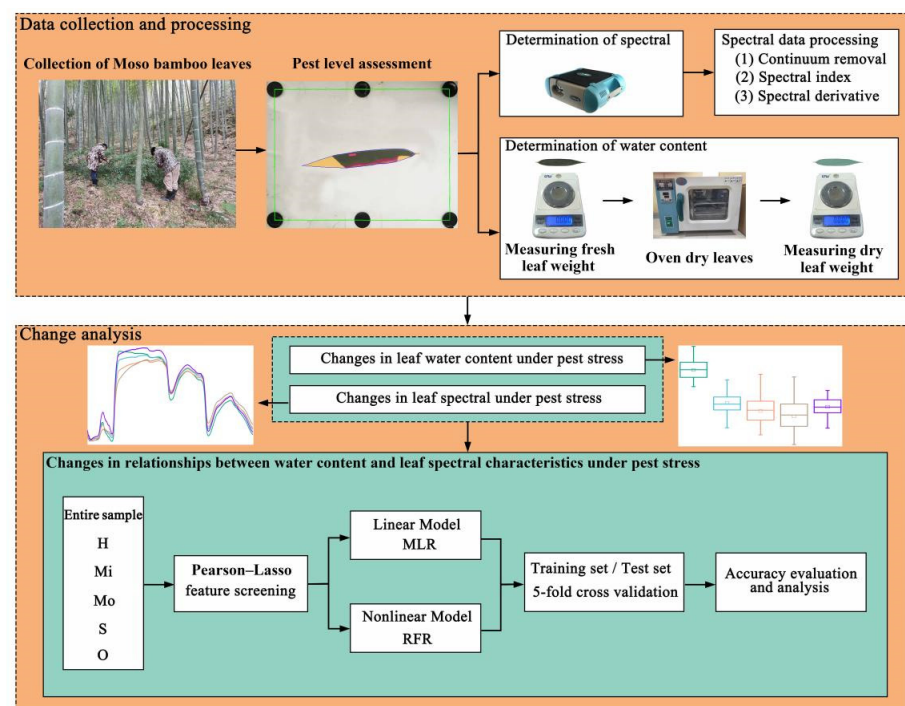


Figure 2. Workflow of changing relationships between water content and leaf spectral features in moso bamboo leaves under PPC stress.

3. Results and Analysis

3.1. Difference in LWC under Different Damage Levels

The LWC changes when the leaf is damaged by PPC. Figure 3 shows that, with increasing damage level, the LWC shows a gradual declining trend overall. However, the rate of decline is substantially slower. The LWC of healthy and damaged leaves varied significantly, whereas the LWC was not significantly different between the Mi-Mo and Mo-S groups (Table 2). The possible factor was that the turgor pressure changed when the leaf was damaged. The pressure of cell water on the cell wall is known as the turgor pressure. When the leaf was not damaged, the turgor pressure was relatively high. However, when moso bamboo leaves start to become damaged, the water content is rapidly lost under the effects of turgor pressure [65]. Therefore, the LWC of healthy and damaged leaves varied significantly. However, with water loss, the leaf turgor pressure continued to decrease, and the water loss rate also slowed down. This may be the reason for the small difference in water content between the damaged leaves. There was no significant difference in LWC among Mi, Mo, and O (Table 2). When moso bamboo is in the off-year stage, most of the nutrients in the maternal bamboo are used for rhizome growth [66], and moso bamboo will show symptoms of water shortage and chlorosis. Therefore, although the bamboo leaves from this period were not affected by PPC, their LWC was highly similar to that of the leaves at the damage level.

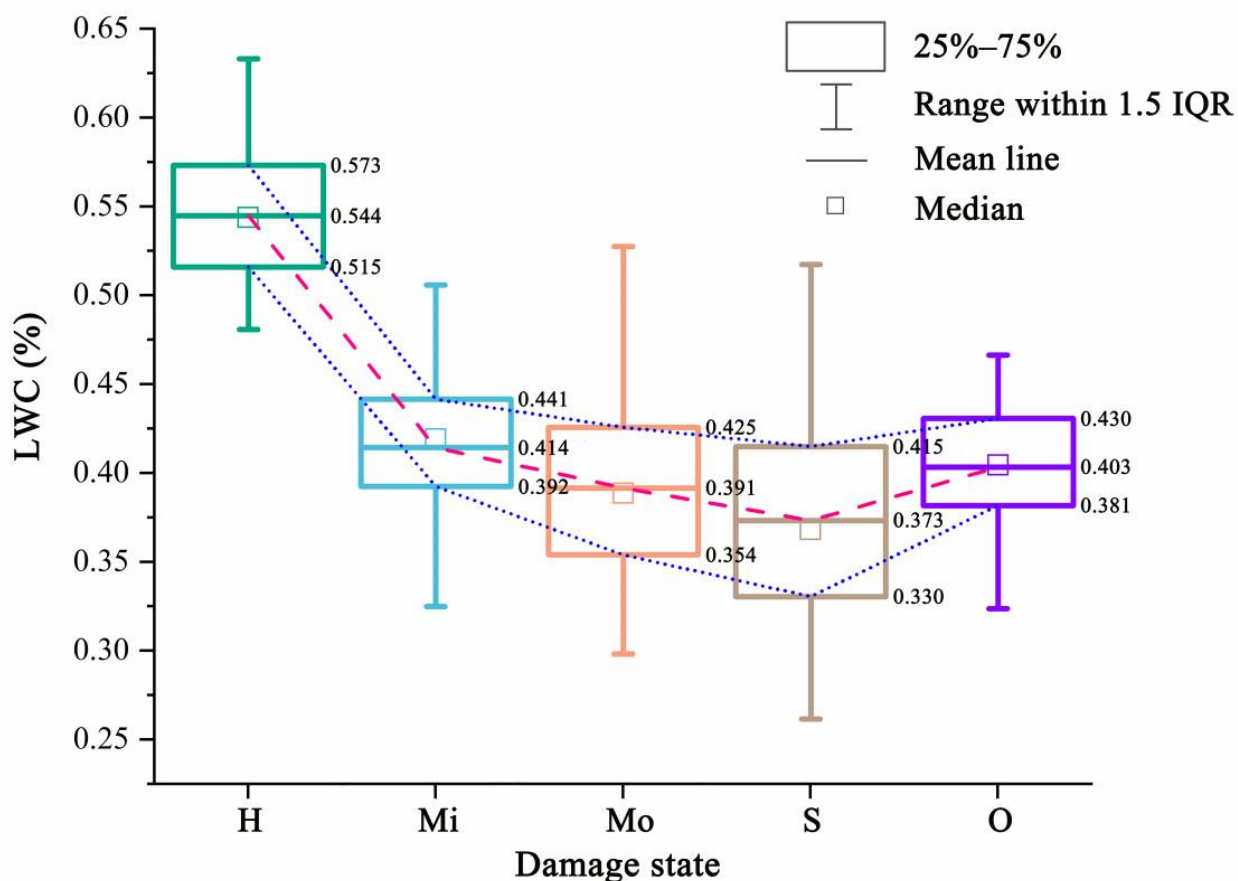


Figure 3. LWC variation trend of moso bamboo leaf under different damage states.

Table 2. ANOVA analysis of LWC of moso bamboo leaves under different damage levels.

Groups	H-Mi	H-Mo	H-S	H-O	Mi-Mo	Mi-S	Mi-O	Mo-S	Mo-O	S-O
<i>p</i> -values	<0.001 **	<0.001 **	<0.001 **	<0.001 **	0.214	<0.001 **	0.968	0.261	0.867	0.004 **

Note: ** indicates $p < 0.01$, showing that the difference is very significant.

3.2. Differences in Leaf Spectra under Different Damage Levels

When moso bamboo leaves are affected by PPC, they show symptoms of water shortage and chlorosis and their spectra change (Figure 4). In the visible region, the green reflectance decreased, and the red reflectance increased as the PPC stress increased. In the NIR region, the reflectance of healthy and damaged leaves were significantly different, showing a decreasing reflectance trend with increasing damage level. In the SWIR region, the reflectance of healthy leaves was generally lower than that of the damaged leaves. The reflectance of off-year leaves was generally higher than that of healthy leaves across the entire range. Compared with damaged leaves, the off-year leaves had higher reflectance in the visible and NIR regions. However, in the SWIR region, they were not distinguishable. In order to further analyze the differences in the spectra of moso bamboo leaves under different damage levels, we conducted a paired *t*-test for the spectra under different damage levels. The results are shown in Table 3, and there are significant differences in the spectra under different damage levels in the visible, NIR, and SWIR regions.

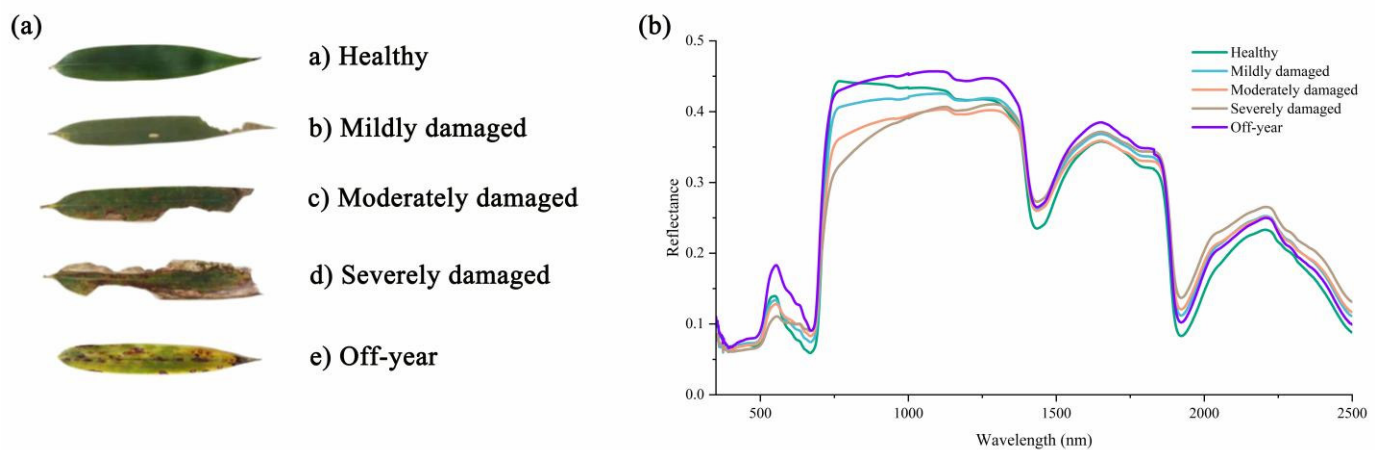


Figure 4. Moso bamboo leaves in different damage states and their spectral information: (a) moso bamboo leaves; (b) spectral information.

Table 3. Paired *t*-test of spectra for leaves with different damage levels.

Pest Level	<i>p</i> -Values		
	Visible Region	NIR Region	SWIR Region
H-Mi	0.004 **	<0.001 **	<0.001 **
H-Mo	<0.001 **	<0.001 **	<0.001 **
H-S	<0.001 **	<0.001 **	<0.001 **
H-O	<0.001 **	<0.001 **	<0.001 **
Mi-Mo	<0.001 **	<0.001 **	<0.001 **
Mi-S	<0.001 **	<0.001 **	<0.001 **
Mi-O	<0.001 **	<0.001 **	<0.001 **
Mo-S	<0.001 **	<0.001 **	<0.001 **
Mo-O	<0.001 **	<0.001 **	<0.001 **
S-O	<0.001 **	<0.001 **	0.010 **

Note: ** indicates $p < 0.01$, showing that the difference is very significant.

3.3. Model Feature Screening Based on the Pearson–Lasso Method

In this study, the LWC of moso bamboo leaves was used as Variable Y, and SCR, SD, and SI were used as Variable X for the Pearson correlation analysis. The features selected are determined based on the absolute value of the correlation coefficient. Given that SCR

and SD have more than 4000 features and there are many features that were significantly related to LWC, their selection process was complex. To this end, SCR and SD were divided into visible, NIR, and SWIR regions. The top correlated features were selected as alternative features in each region. In comparison, the SI number was relatively low, and all the indices that were significantly associated with the LWC could be selected as alternative features. Lasso regression produces items with a regression coefficient of zero under the constraint of the model properties. When selecting features, removing these items can significantly reduce collinearity between features [67]. We randomly divided all the alternative features into a modeling set and a validation set in a 7:3 ratio and eliminated features with strong collinearity for feature optimization.

The correlation between the spectral features and LWC was different for leaves under different damage levels (Figure 5a–l). In terms of quantity, there were more features significantly related to the LWC of the entire sample, H, and S (3207, 2762, and 2322, respectively). Meanwhile, there were relatively few features significantly related to the LWC of Mi, Mo, and O (1295, 627, and 817, respectively). The LWC of the entire sample, H, and S had a strong correlation with the features. The mean Pearson coefficients were 0.187, 0.281, and 0.231, respectively. The correlation between LWC and features of Mi, Mo, and O was relatively low. The mean Pearson coefficients were 0.148, 0.115, and 0.159, respectively. According to these principles of feature selection, the results are as follows, for the entire sample: SCR_{367nm}, SCR_{665nm}, SCR_{1928nm}, SCR_{2033nm}, SD_{520nm}, SD_{1939nm}, SD_{2062nm}, SAI₁₆₆₀; H: SCR_{765nm}, SCR_{2117nm}, SD_{422nm}, SD_{1836nm}, SD_{2038nm}, CI, VOG, NDWI₁, NDWI₂₁₃₀; Mi: SCR_{1280nm}, SCR_{2254nm}, SD_{436nm}, SD_{1763nm}, SD_{2265nm}, SD_{2316nm}, SIWSI, TM57; Mo: SCR_{1703nm}, SCR_{2272nm}, SD_{1918nm}, SD_{1948nm}, SD_{2249nm}, SD_{2466nm}, SAI₉₇₀; S: SD_{1222nm}, SD_{1742nm}, SD_{1811nm}, SD_{2260nm}, SD_{2312nm}, MCARI, LWI, SAI₁₂₀₀; O: SCR_{706nm}, SCR_{2223nm}, SD_{399nm}, SD_{687nm}, SD_{1182nm}, DDI, MSI₂, and SAI₁₂₀₀.

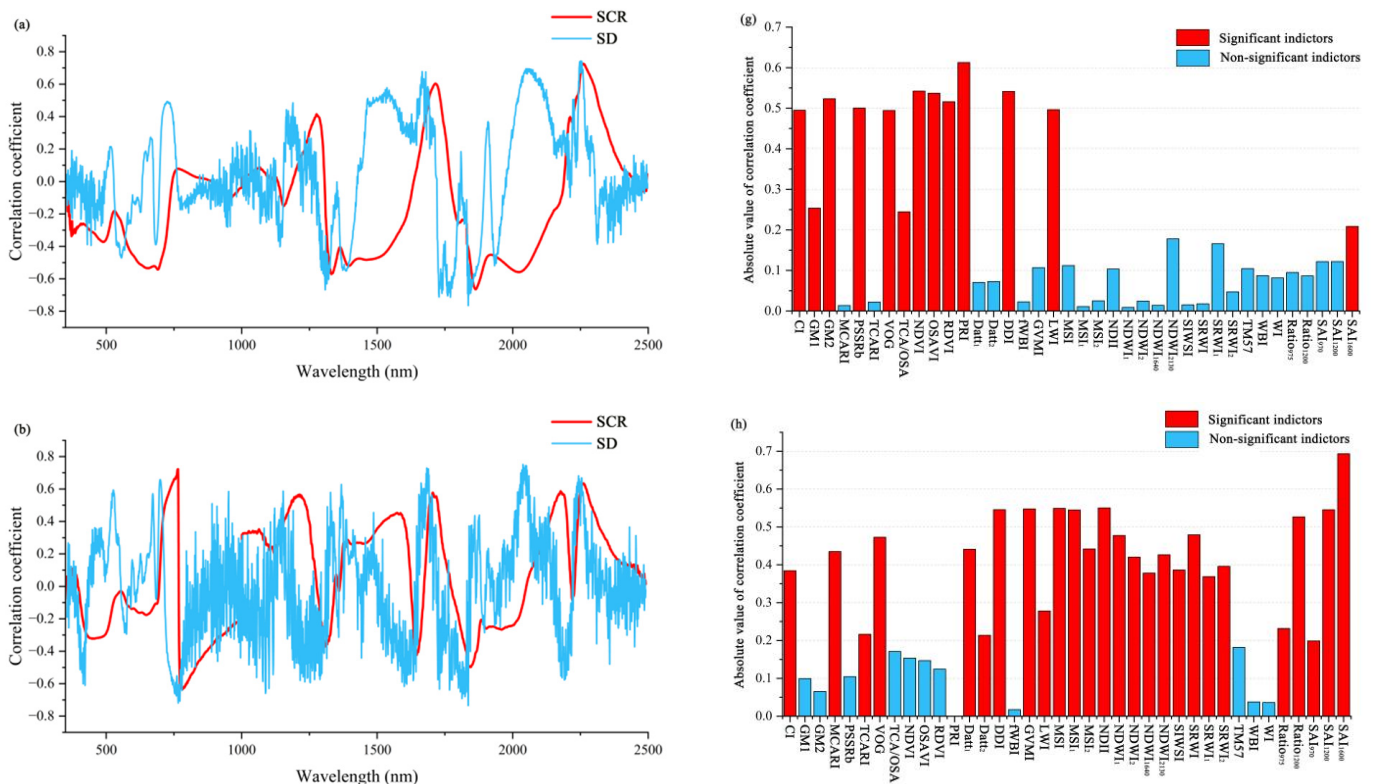


Figure 5. Cont.

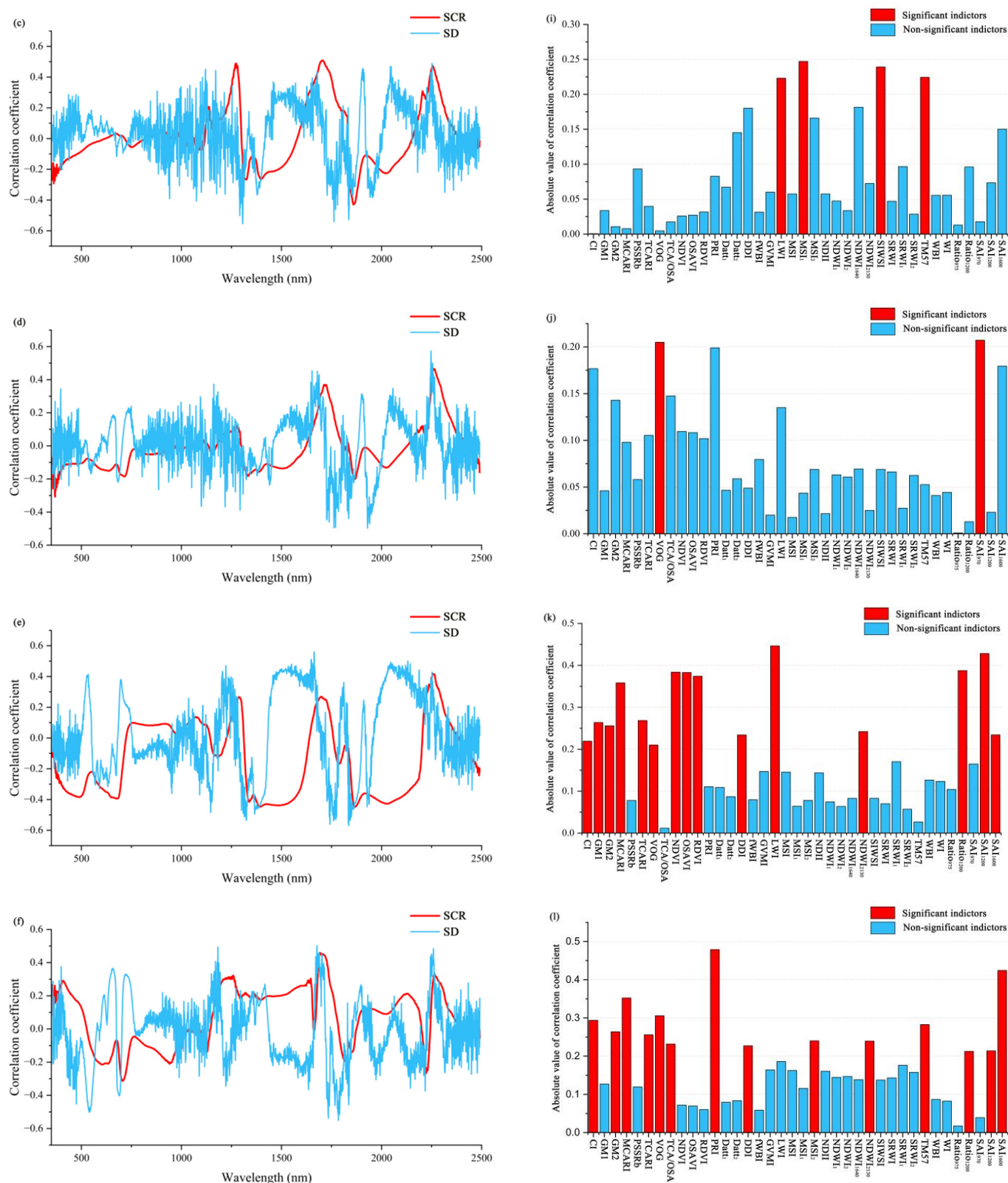


Figure 5. Correlation between spectral features and LWC. (a–f) Correlations between spectral data (SCR and SD) and LWC in the entire sample and in H, Mi, Mo, S, and O states, respectively. (g–l) Correlations between spectral index and LWC in the entire sample and in H, Mi, Mo, S, and O states, respectively.

It can be seen that the bands involved in response features of leaf water content at different damage levels are distributed differently in the visible, NIR, and SWIR regions. The bands involved in response features of healthy moso bamboo leaves were distributed in all regions (visible, NIR, and SWIR), which is due to different healthy leaves with different colors and cell structures, and due to the ability of water to absorb the spectrum, resulting in significant differences in spectra in the visible, NIR, and SWIR regions. For mildly damaged leaves, as they begin to become damaged, the leaf water is rapidly lost, and the ability of water to absorb the spectrum varies widely among leaves. Therefore, the bands involved in response features were mostly distributed in the SWIR region. But the color and cell structure of the leaves were also changed after being bitten by pests, so the bands involved in response features were also partly distributed in the visible and NIR regions. Moderately and severely damaged moso bamboo leaves have been infested with insects for a longer period of time, and the color and cell structure of the leaves will not be very different; therefore, the bands involved in response features were mainly concentrated in the SWIR region. For off-year moso bamboo leaves, they were mainly affected by the lack of nutrients and, as a result, the phenomena of leaf yellowing and water deficiency appeared. In addition, the cell structure was changed; therefore, the bands involved in response features were distributed in all regions (visible, NIR, and SWIR).

3.4. Model Construction and Relationship Analysis between LWC and Spectral Features of Moso Bamboo Leaves

3.4.1. LWC Estimation for Leaves from the Entire Sample and Leaves with Different Damage Levels

We substituted the features selected into MLR and RFR models, respectively. We then used fivefold cross-validation to estimate the LWC of the leaf samples under different damage levels, with the model evaluation indicators of the R^2 and RMSE. Figure 6 shows the effect of MLR and RFR on estimating the LWC of bamboo leaves for the entire sample and different damage levels. Most points were within the 95% confidence ellipse, and p -values for both models were less than 0.01. The estimated R^2 values of MLR for the LWC of the entire sample, H, Mi, Mo, S, and O were 0.761, 0.803, 0.620, 0.482, 0.675, and 0.598, respectively. The RMSE were 0.038, 0.014, 0.022, 0.041, 0.035, and 0.022, respectively. The estimated R^2 of the RFR for the LWC of the entire sample, H, Mi, Mo, S, and O were 0.790, 0.819, 0.689, 0.562, 0.712, and 0.666, respectively. The RMSE was 0.036, 0.013, 0.020, 0.038, 0.033, and 0.020, respectively. The estimation accuracy of the two models for the LWC of H, Mi, Mo, S, and O first decreased and then increased, and the performance of RFR was generally better than that of MLR.

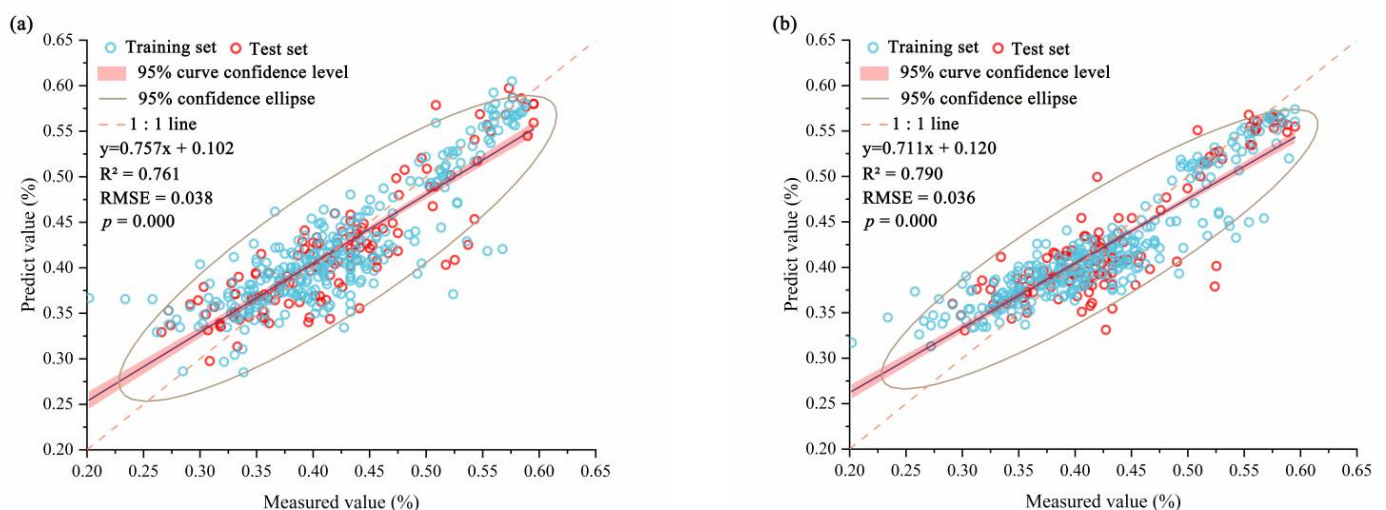


Figure 6. Cont.

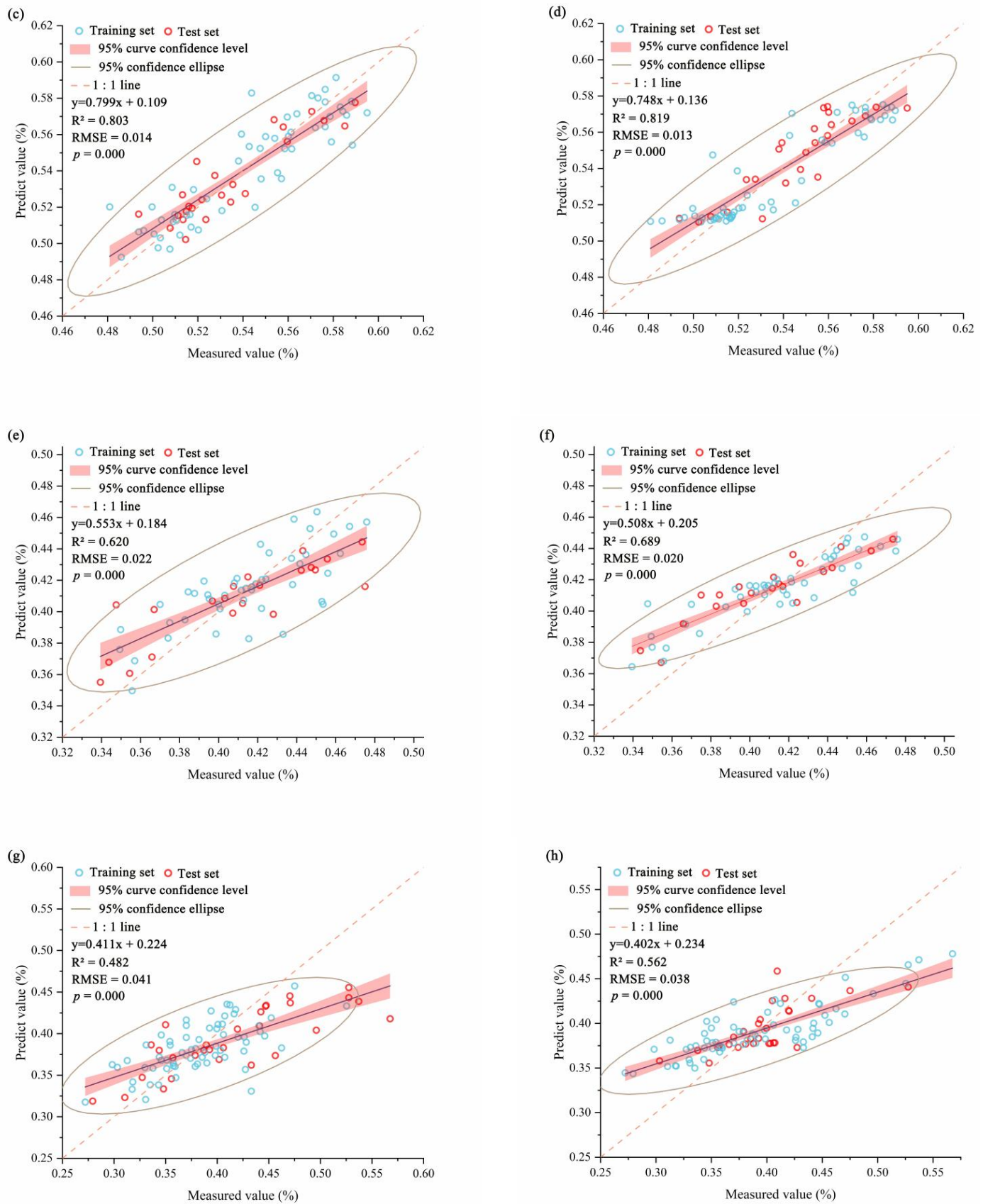


Figure 6. Cont.

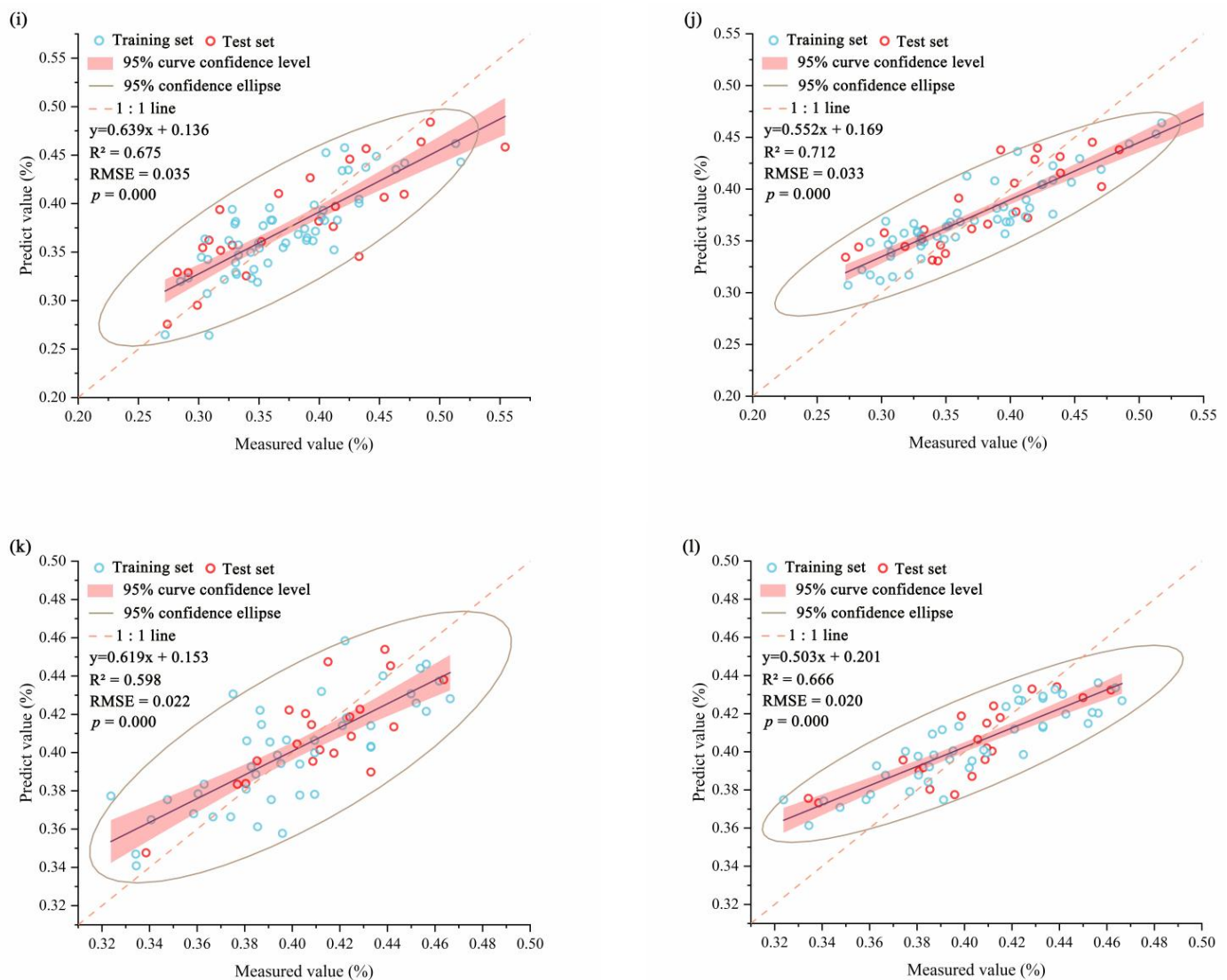


Figure 6. Estimated LWC of bamboo leaves in different damage states: (a) entire sample, MLR model; (b) entire sample, RF model; (c) H-MLR; (d) H-RFR; (e) Mi-MLR; (f) Mi-RFR; (g) Mo-MLR; (h) Mo-RFR; (i) S-MLR; (j) S-RFR; (k) O-MLR; (l) O-RFR. Multiple linear regression (MLR), random forest regression (RFR).

3.4.2. Paired t -Test of LWC Estimation Indices for Entire Leaf Samples and Leaves with Different Damage Levels

To quantitatively analyze the estimation effect of the model on the LWC of the leaves from the entire sample and leaves at different damage levels, we conducted a paired t -test on the results of five trials of MLR and RFR. Table 4 shows that for the MLR estimation method, the RMSE was not significantly different between Mi and O. For the RFR estimation method, the R^2 and RMSE were not significantly different between Mi and O. The two methods for the other groups were significantly different. This shows that PPC has a pronounced effect on the estimation of LWC. The estimation effect of MLR and RFR on LWC showed that healthy leaves were significantly better than the entire sample leaves, and the leaves from the entire sample were significantly better than the damaged and off-year leaves (Table 4). This indicates that the damaged and off-year leaves would reduce the estimation accuracy of the LWC of the entire sample.

Table 4. Paired *t*-test of LWC estimation indices for leaves from the entire sample and leaves with different damage levels.

Pest Level	MLR				RFR			
	R ²		RMSE		R ²		RMSE	
	t	p	t	p	t	p	t	p
H-Mi	12.246	<0.001 **	−18.480	<0.001 **	12.982	<0.001 **	−19.382	<0.001 **
H-Mo	53.281	<0.001 **	−123.195	<0.001 **	25.713	<0.001 **	−64.062	<0.001 **
H-S	9.684	0.001 **	−36.381	<0.001 **	18.274	<0.001 **	−72.242	<0.001 **
H-O	20.670	<0.001 **	−28.173	<0.001 **	8.323	<0.001 **	−11.730	<0.001 **
H-entire sample	3.720	0.020 *	−66.237	<0.001 **	4.616	<0.001 **	−103.505	<0.001 **
Mi-Mo	11.191	<0.001 **	−45.079	<0.001 **	9.315	<0.001 **	−35.650	<0.001 **
Mi-S	−3.064	0.038 *	−18.605	<0.001 **	−2.840	0.047 *	−55.985	<0.001 **
Mi-O	3.596	0.023 *	−1.955	0.122	0.722	0.510	0.119	0.911
Mi-entire sample	−22.073	<0.001 **	−114.789	<0.001 **	−7.393	0.002 **	−33.987	<0.001 **
Mo-S	−16.175	<0.001 **	9.454	0.001 **	−16.744	<0.001 **	11.228	<0.001 **
Mo-O	−7.501	0.002 **	42.582	<0.001 **	−14.789	<0.001 **	67.952	<0.001 **
Mo-entire sample	−32.577	<0.001 **	5.665	0.005 **	−38.641	<0.001 **	6.230	0.003 **
S-O	7.667	0.002 **	22.978	<0.001 **	2.940	0.042 *	28.670	<0.001 **
S-entire sample	−7.482	0.002 **	−5.114	0.007 **	−12.852	<0.001 **	−9.360	0.001 **
O-entire sample	−22.746	<0.001 **	−63.114	<0.001 **	−9.007	0.001 **	−36.475	<0.001 **

Note: * indicates $p < 0.05$, showing that the difference is significant; ** indicates $p < 0.01$, showing that the difference is very significant.

3.4.3. Paired *t*-Test for MLR and RFR Models

To analyze the difference between MLR and RFR in estimating the LWC, we conducted a paired *t*-test on the results from the two methods under the same damage level. Table 5 shows that there is no significant difference between R² and RMSE estimated by the two methods for the LWC of healthy leaves. However, there is a significant difference between R² and RMSE as estimated by the two methods for the LWC of damaged and off-year leaves. The estimation effect of RFR is significantly stronger than that of MLR. MLR can reflect the simple linear relationship between variables, whereas RFR can reflect the complex nonlinear relationship between variables. MLR and RFR were not significantly different in estimating the LWC of healthy leaves. MLR was able to estimate the LWC effectively, indicating that the relationship between LWC and features of healthy leaves tended to be a simple linear relationship. In contrast, RFR was significantly more effective than MLR in estimating the LWC of damaged and off-year leaves. This indicates that the relationship between LWC and features can no longer be expressed by a simple linear relationship. Therefore, the relationship between LWC and features of damaged and off-year leaves tends to be more complex.

Table 5. Paired *t*-test of MLR and RFR models.

Pest Level	MLR-RFR			
	R ²		RMSE	
	t	p	t	p
H	−1.427	0.227	1.636	0.177
Mi	−3.936	0.017 *	3.945	0.017 *
Mo	−4.171	0.006 **	4.194	0.006 **

Table 5. Cont.

Pest Level	MLR-RFR			
	R ²		RMSE	
	t	p	t	p
S	−5.157	0.007 **	5.247	0.006 **
O	−9.980	0.001 **	9.478	0.001 **
Entire sample	−17.252	<0.001 **	15.442	<0.001 **

Note: * indicates $p < 0.05$, showing that the difference is significant; ** indicates $p < 0.01$, showing that the difference is very significant.

4. Discussion

4.1. Leaf Loss Rate, Die-Off Rate, and LWC

To investigate the effects of leaf loss and die-off rates on LWC, we analyzed their correlation. As shown in Figure 7, the sum of the leaf loss rate and leaf die-off rate had the highest correlation with LWC. This was followed by the correlation between leaf die-off rate and LWC. The correlation between leaf loss rate and LWC was the lowest.

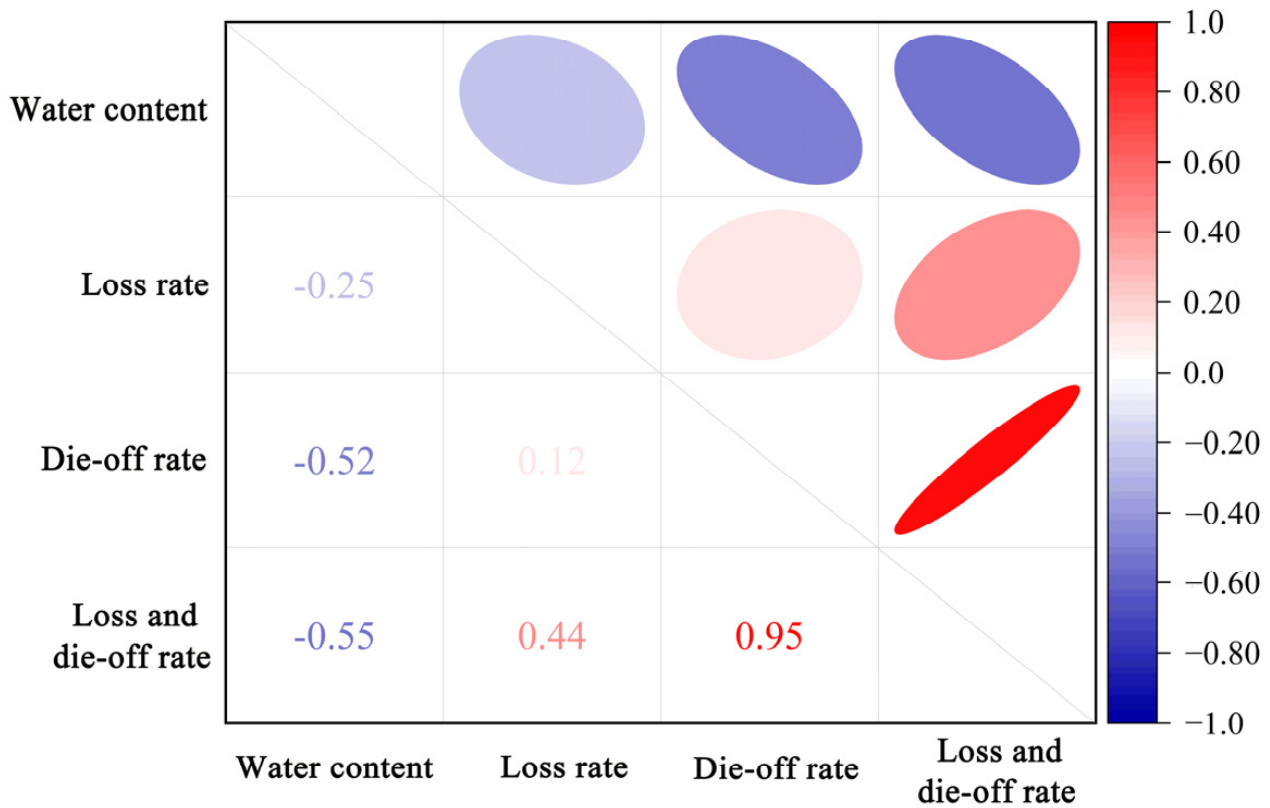


Figure 7. Correlation between LWC, rate of leaf loss, rate of leaf die-off, and their interaction.

Water is directly involved in the transformation and synthesis of various substances in plants and is an indispensable factor for maintaining cell turgor pressure and balancing plant temperature. When leaves are stressed by PPC, their cell walls, cell membranes, and other tissues are damaged and internal water is lost. This may result in cellular water deficiency, reduced turgor pressure, reduced stomatal conductance, and a slower transpiration rate [68]. If the leaves are in a suitable external environment, slow transpiration can maintain the normal temperature of the leaf without permanent damage. When the damaged part of the leaf gradually heals, the leaf water loss rate slows down. Vegetation has a certain water compensation mechanism that can alleviate the damage caused by

leaf water loss. Even when the leaf loss rate increased, the LWC of the entire leaf did not substantially change (Figure 8a). If the leaves are exposed to high temperatures or direct sunlight after being eaten by PPC, the leaf water loss rate is relatively rapid, and the water in the roots is difficult to supplement in time. The transpiration of the leaves then becomes weak and the excess heat on the leaves cannot be removed. Parts of the leaf become completely desiccated with dead spots appearing (Figure 8b). This leads to a water deficit in the entire leaf. The appearance of dead spots on the leaves implies greater water loss, which may be the reason why the die-off rate has a higher correlation with LWC. The rate of leaf loss and leaf die-off jointly caused a reduction in LWC. However, there was no significant correlation (Figure 7), indicating that they have their own independent contributions to the reduction in LWC. Therefore, the interaction between the rate of leaf loss and leaf die-off had the most pronounced impact on LWC.

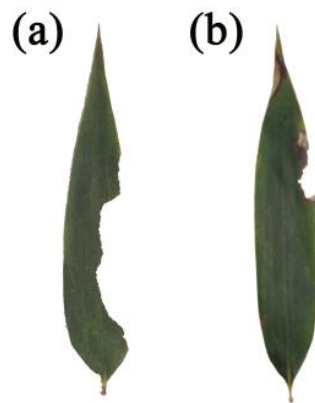


Figure 8. Leaves in different external environments: (a) the leaf gradually recovered after being bitten by insects; (b) the leaf was completely dehydrated in some parts and dead spots appeared after being bitten by insects.

4.2. Inconsistent Accuracy of LWC Estimation under Different Damage Levels

Leaf reflectance in the visible region was predominantly influenced by photosynthetic pigments. After being stressed by PPC, the leaves suffer from water shortages. Their transpiration efficiency also declines, which means that the necessary pigment synthesis materials cannot be transported to the leaves. Therefore, the leaf reflectance changes in the visible region. Leaf reflectance in the NIR region was predominantly influenced by its structure. When the leaf is stressed by PPC, its structure is damaged, and the internal scattering of light inside the leaf is weakened [69–71]. Thus, the reflectance of the leaf changes in the NIR region. Leaf reflectance in the SWIR region is predominantly affected by water, and water loss may lead to changes in the SWIR region. The leaf spectra in the visible, NIR, and SWIR regions were different under different damage levels. The number of response features and degree of response changed with different damage levels. Therefore, the estimation accuracy of LWC differed under different damage levels.

When the leaf was stressed by PPC, the water loss rate of the damaged section occurred faster than that of the undamaged section, and the water content near the leaf vein was higher than that of the other sections. Therefore, the distribution of water in the leaves has pronounced spatial heterogeneity. Physical and chemical parameters, such as chlorophyll and nitrogen content, also show pronounced spatial heterogeneity after being stressed by pests [72]. This spatial heterogeneity leads to high complexity in the leaf spectral curve and increases the difficulty in estimating the LWC. There was almost no spatial heterogeneity in the healthy leaves, and the spectral curves of different parts of the leaf showed little difference. The spatial heterogeneity of the damaged and off-year leaves was relatively high, and the spectral confusion was severe (Figure 9). In this study, we used spectral information as the basis for LWC estimation, and a high degree of spectral confusion significantly affected the accuracy of the LWC estimation.

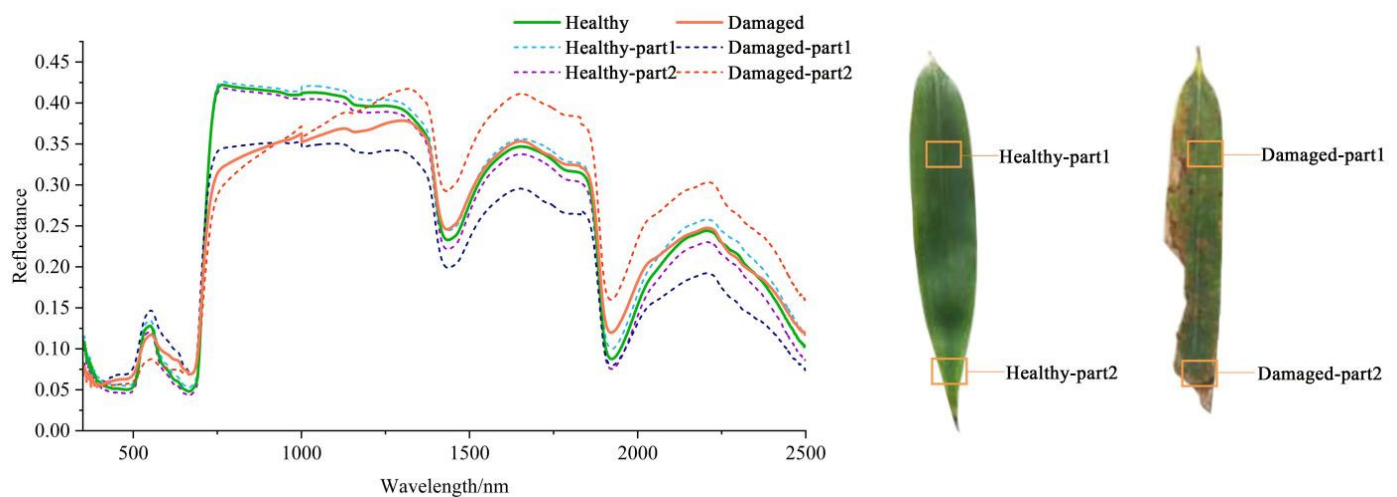


Figure 9. Spectral curve difference caused by spatial heterogeneity of the leaves. The solid green line is the average of the spectral curves of Healthy-part1 and Healthy-part2. The solid orange line is the average of the spectral curves of Damaged-part1 and Damaged-part2.

4.3. Correlation Analysis of LWC and Features under Different Damage Levels

To further examine changes in the correlation between the LWC and features with the increase in damage level, we calculated the correlation coefficients between the LWC and all features under different damage levels and analyzed their changes. Figures 10 and 11 showed that the number of features significantly related to the LWC of healthy leaves was 2762, accounting for approximately 64% of the total features. The maximum correlation coefficient reached approximately 0.75. Therefore, the correlation coefficient between the LWC and the features of healthy leaves was generally high. The correlation coefficient between features and LWC of severely damaged leaves was 2322, accounting for more than 50% of the total features. However, the maximum value was less than 0.6, with a larger gap than that of healthy leaves. The correlation coefficients between features and LWC of Mi, Mo, and O were generally low. The number of significantly correlated features was small, and the maximum value did not exceed 0.5. In general, with an increase in the level of damage, the number and significance of features significantly related to LWC first decreased and then increased. The correlation between LWC and features of healthy leaves was significantly higher than that of damaged and off-year leaves. The spectra of moso bamboo leaves would change when they were under PPC stress or in the off-year stage, the correlation between LWC and features would worsen, and the estimation accuracy of the model would decrease. Therefore, when there is a less strong relationship between LWC and features, it indicates that PPC is present or that the moso bamboo is in the off-year stage.

4.4. Measured Non-Imaging Hyperspectral Data for Research and Application

Measured non-imaging spectra and satellite images are important remote sensing data. Although their data manifestations are different, their databases are spectroscopic, so the two sets of data have a high coincidence in some waveband ranges. Fu et al. [73] researched the biochemical composition of tobacco using measured non-imaging hyperspectra and matched them with Landsat 8 images to improve the accuracy of the model. This had considerable theoretical importance and practical application value for determining the quality of tobacco. Chu et al. [74] used a measured non-imaging hyperspectrum for fine classification of tree species and concluded that non-imaging spectral research could provide theoretical support for remote sensing spectral imaging research and applications. Therefore, measured non-imaging spectral data can be used as multisource data to perform spectral matching with satellite images and can provide theoretical support for the research and application of satellite images. In this study, measured non-imaging hyperspectral data were used to investigate the microscopic mechanisms of biochemical components and

pest information to explore the change mechanism in plant biochemical components and leaf spectra when PPC is present. The quantitative relationships between them were also clarified, which can lay a foundation for real-time, rapid, and large-area monitoring and, using satellite images, can provide early warning systems for pests.

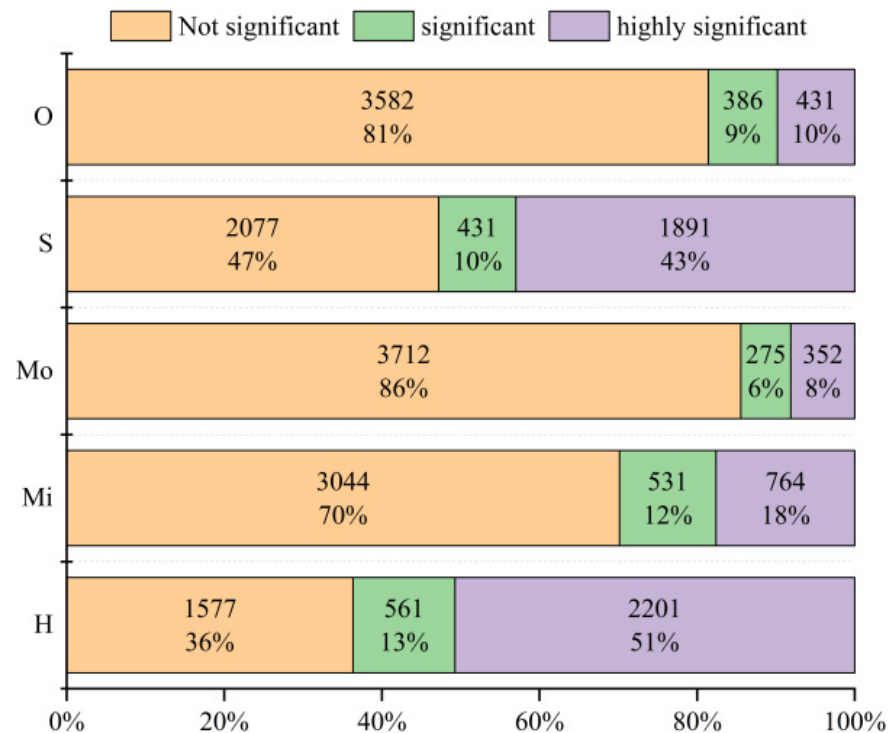


Figure 10. Significant changes in feature indices under different pest levels.

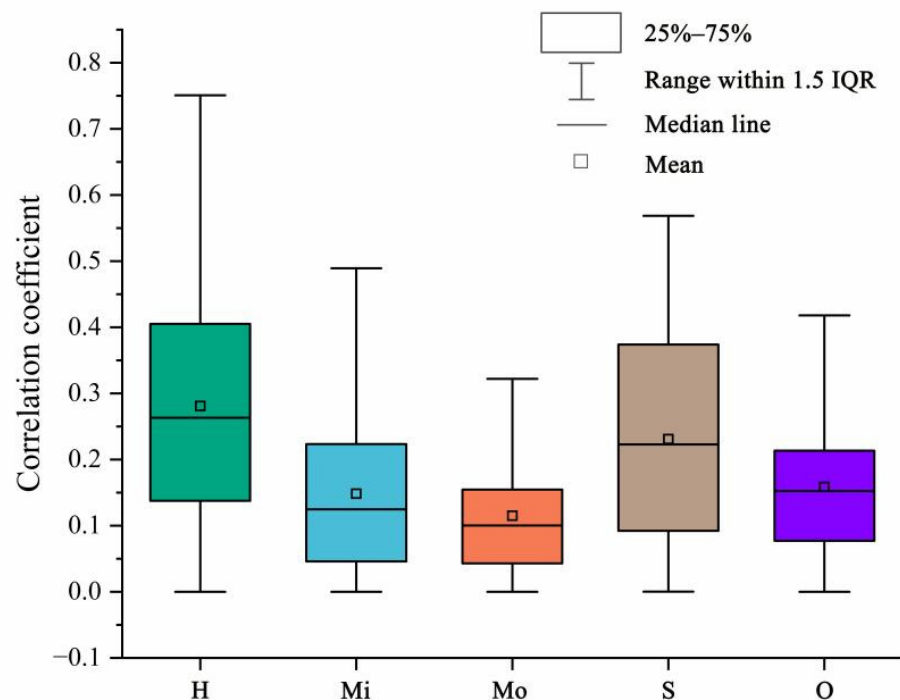


Figure 11. Changing trend of correlation between characteristic indices and leaf water content under different pest levels.

4.5. Study of the Change Mechanism of LWC and Spectra to Support Pest Detection

When moso bamboo suffers from pest stress, its biochemical components and leaf spectra will be changed. It is of great significance for pest detection to study the change mechanism and regularity of biochemical components and spectral features under different damage levels. Previous researchers have investigated the change mechanism and regularity between chlorophyll [70], nitrogen [10] and spectral features under different pest levels, which have laid the foundation for pest detection. In this paper, we started with LWC to explore the change mechanism and regularity, which is expected to aid with pest detection. The correlation between response features and LWC is different and the prediction effect of LWC is also different under different pest levels. Therefore, we may not be able to build an accurate pest detection model using these features; nevertheless, change in spectral features exhibits parity with LWC and pest stress damage and may provide a robust predictive tool for developing a remote sensing model for pest stress survey in the targeted region.

5. Conclusions

In this study, we used the measured spectra and LWC of moso bamboo leaves as the main datasets and used the Pearson–Lasso algorithm to screen the response features. We also established an MLR and RFR estimation model for LWC. We analyzed the relationship between LWC and spectral features of moso bamboo leaves under PPC stress and their changes by comparing the results of feature screening and model estimation. The following conclusions were drawn.

- (1) LWC and spectra of moso bamboo changed under PPC stress, and the number and significance of features associated with the LWC of moso bamboo leaves varied under different damage levels. With increasing damage levels, the number and significance of features significantly related to LWC first decreased and then increased. The correlation between LWC and features of healthy leaves was significantly higher than that of damaged and off-year leaves.
- (2) The most effective estimation model for samples under different damage levels was RFR, achieving model accuracy as follows: for the entire sample ($R^2 = 0.790$, RMSE = 0.036), for H ($R^2 = 0.819$, RMSE = 0.013), for Mi ($R^2 = 0.689$, RMSE = 0.020), for Mo ($R^2 = 0.562$, RMSE = 0.038), for S ($R^2 = 0.712$, RMSE = 0.033), and for O ($R^2 = 0.666$, RMSE = 0.020).
- (3) The estimated effect of LWC under different damage levels was significantly different. The estimation effect of MLR and RFR for different damage levels showed a trend of healthy leaves being significantly better than leaves from the entire sample, and the leaves from the entire sample were significantly better than damaged and off-year leaves. This indicates that PPC damage had a pronounced effect on the estimation of the LWC. Damaged and off-year leaves reduced the estimation accuracy of the LWC from the entire sample.
- (4) For healthy leaves, there was no significant difference between the estimation effects of MLR and RFR. MLR was effective in estimating the LWC. For damaged and off-year leaves, the estimation effect of RFR was significantly better than that of MLR. The estimation effect of MLR was at a lower level. This indicated that the relationship between LWC and features of healthy leaves tended to be a simple linear relationship. Meanwhile, the relationship between LWC and features of damaged and off-year leaves tended to be relatively complex.

In summary, we used the Pearson–Lasso method to screen features and RFR to estimate the LWC of bamboo leaves, which has a positive effect. By analyzing the relationship between leaf spectra and PPC occurrence, we found that leaf spectra differed when leaves were subjected to different damage levels. By analyzing the level of correlation between the LWC and spectral features under different damage levels, as well as the model estimation effect, we also found that when the relationship between LWC and spectral features of moso bamboo leaves tends to be disordered, this indicates that moso bamboo is in an off-year

stage or that PPC is present. Although we have not explored the direct response features of pest stress, the change in spectral features exhibits parity with LWC and pest stress damage, which may provide a robust predictive tool for developing a remote sensing model for pest stress survey in the targeted region. In terms of limitations, we only explored the relationship between measured spectra and LWC of moso bamboo leaves under pest stress, without further discussing the docking relationship between measured spectra and satellite images. In the future, we will further study the relationship between them.

Author Contributions: Conceptualization, Z.X. and B.L.; methodology, Z.X., B.L., H.Y. and H.Z.; software, Y.L. and A.H.; validation, X.G., Z.L. (Zenglu Li) and H.Y.; data curation, X.H. and B.L.; writing—original draft preparation, Z.X. and B.L.; writing—review and editing, Z.X., L.W. and Z.L. (Zhikai Liu); visualization, H.Z., X.G. and Z.L. (Zenglu Li). All authors have read and agreed to the published version of the manuscript.

Funding: This research was supported by the National Natural Science Foundation of China, grant number 42071300; the Fujian Province Natural Science Foundation Project, grant number 2020J01504; the China Postdoctoral Science Foundation, grant number 2018M630728; the Open Fund of Fujian Provincial Key Laboratory of Resources and Environment Monitoring and Sustainable Management and Utilization, grant number ZD202102; the Program for Innovative Research Team in Science and Technology in Fujian Province University, grant number KC190002; the Research Project of Jinjiang Fuda Science and Education Park Development Center, grant number 2019-JJFDKY-17; and the Open Fund of University Key Lab for Geomatics Technology and Optimized Resource Utilization in Fujian Province, grant number fafugeo201901.

Institutional Review Board Statement: Not applicable.

Informed Consent Statement: Not applicable.

Data Availability Statement: Data and associated codes are available from the corresponding author upon reasonable request.

Acknowledgments: We are grateful to the Forestry Bureau of Shunchang County for its help with this work. We would like to thank Zhaoquan Zhong and Xianyun Lin for their help with the field experiment.

Conflicts of Interest: The authors declare no conflict of interest.

References

1. Apan, A.; Held, A.; Phinn, S.; Markley, J. Detecting sugarcane ‘orange rust’ disease using EO-1 Hyperion hyperspectral imagery. *Int. J. Remote Sens.* **2004**, *25*, 489–498. [\[CrossRef\]](#)
2. Goławska, S.; Krzyżanowski, R.; Łukasik, I. Relationship between aphid infestation and chlorophyll content in Fabaceae species. *Acta Biol. Cracov. Ser. Bot.* **2010**, *52*, 76–80. [\[CrossRef\]](#)
3. Feng, Z.H.; Wang, L.Y.; Yang, Z.Q.; Zhang, Y.Y.; Li, X.; Song, L.; He, L.; Duan, J.Z.; Feng, W. Hyperspectral monitoring of powdery mildew disease severity in wheat based on machine learning. *Front. Plant Sci.* **2022**, *13*, 828454. [\[CrossRef\]](#) [\[PubMed\]](#)
4. Macedo, T.B.; Weaver, D.K.; Peterson, R.K.D. Characterization of the impact of wheat stem sawfly, *Cephus cinctus* Norton, on pigment composition and photosystem II photochemistry of wheat heads. *Environ. Entomol.* **2006**, *35*, 1115–1120. [\[CrossRef\]](#)
5. Errard, A.; Ulrichs, C.; Kühne, S.; Mewis, I.; Drungowski, M.; Schreiner, M.; Baldermann, S. Single-versus multiple-pest infestation affects differently the biochemistry of tomato (*Solanum lycopersicum* ‘Ailsa Craig’). *J. Agric. Food Chem.* **2015**, *63*, 10103–10111. [\[CrossRef\]](#)
6. Polyakova, L.V.; Gamayunova, S.G.; Zhurova, P.T.; Litvinenko, V.I. Biochemical specifics of English oak trees with dry crown. *Contemp. Probl. Ecol.* **2015**, *8*, 885–891. [\[CrossRef\]](#)
7. Liang, S.X.; Qian, S.S.; Hei, Z.H. Life history of the moth *Pantana phyllostachysae* and its control. *Chin. J. Appl. Entomol.* **2004**, *41*, 464–467.
8. Xu, M.; Liu, R.; Chen, J.M.; Liu, Y.; Shang, R.; Ju, W.; Wu, C.; Huang, W. Retrieving leaf chlorophyll content using a matrix-based vegetation index combination approach. *Remote Sens. Environ.* **2019**, *224*, 60–73. [\[CrossRef\]](#)
9. Li, M.; Zhu, X.; Li, W.; Tang, X.; Yu, X.; Jiang, Y. Retrieval of nitrogen content in apple canopy based on unmanned aerial vehicle hyperspectral images using a modified correlation coefficient method. *Sustainability* **2022**, *14*, 1992–2007. [\[CrossRef\]](#)
10. Xu, Z.H.; Yu, H.; Li, B.; Hao, Z.B.; Li, Y.F.; Xiang, S.Y.; Huang, X.Y.; Li, Z.L.; Guo, X.Y. Changing Relationships between Nitrogen Content and Leaf Spectral Characteristics of Moso Bamboo Leaves under *Pantana phyllostachysae* Chao Stress. *Forests* **2022**, *13*, 1752. [\[CrossRef\]](#)

11. Camino, C.; Calderón, R.; Parnell, S.; Dierkes, H.; Chemin, Y.; Román-Écija, M.; Montes-Borrego, M.; Landa, B.B.; Navas-Cortes, J.A.; Zarco-Tejada, P.J.; et al. Detection of *Xylella fastidiosa* in almond orchards by synergic use of an epidemic spread model and remotely sensed plant traits. *Remote Sens. Environ.* **2021**, *260*, 112420. [[CrossRef](#)] [[PubMed](#)]
12. Zhang, L.; Zhang, H.; Niu, Y.; Han, W. Mapping maize water stress based on UAV multispectral remote sensing. *Remote Sens.* **2019**, *11*, 605. [[CrossRef](#)]
13. Afzal, A.; Mousavi, S.F. Estimation of moisture in maize leaf by measuring leaf dielectric constant. *Int. J. Agric. Biol.* **2008**, *10*, 66–68.
14. Lian, L.; Wang, Z.X.; Gao, Y.L.; Shi, Y.Q.; Yang, Y.Q.; Li, P.; Yusun, T.S.J. Hyperspectral estimation model of water content in coronal layer of jujube damaged by *Tetranychus truncatus*. *Southwest China J. Agric. Sci.* **2020**, *33*, 2524–2529.
15. Niu, T.; Alishir, K.; Umut, H.; Philipp, G.; Birgit, K.; Abdimijit, A.; Suriyegul, H.; Liu, G.L. Characteristics of *Populus euphratica* leaf water and chlorophyll contents in an arid area of Xinjiang, Northwest China. *Chin. J. Ecol.* **2012**, *31*, 1353–1360.
16. Tucker, C.J. Remote sensing of leaf water content in the near infrared. *Remote Sens. Environ.* **1979**, *10*, 23–32. [[CrossRef](#)]
17. Datt, B. Remote Sensing of Water Content in Eucalyptus Leaves. *Aust. J. Bot.* **1999**, *47*, 909. [[CrossRef](#)]
18. Danson, F.M.; Bowyer, P. Estimating live fuel moisture content from remotely sensed reflectance. *Remote Sens. Environ.* **2004**, *92*, 309–321. [[CrossRef](#)]
19. Hunt, E.R.; Rock, B.N.; Nobel, P.S. Measurement of leaf relative water content by infrared reflectance. *Remote Sens. Environ.* **1987**, *22*, 429–435. [[CrossRef](#)]
20. Jacquemoud, S.; Baret, F. PROSPECT: A model of leaf optical properties spectra. *Remote Sens. Environ.* **1990**, *34*, 75–91. [[CrossRef](#)]
21. Carter, G.A. Primary and secondary effects of water content on the spectral reflectance of leaves. *Am. J. Bot.* **1991**, *78*, 916–924. [[CrossRef](#)]
22. Danson, F.M.; Steven, M.D.; Malthus, T.J.; Clark, J.A. High-spectral resolution data for determining leaf water content. *Int. J. Remote Sens.* **1992**, *13*, 461–470. [[CrossRef](#)]
23. Aldakheel, Y.Y.; Danson, F.M. Spectral reflectance of dehydrating leaves: Measurements and modelling. *Int. J. Remote Sens.* **1997**, *18*, 3683–3690. [[CrossRef](#)]
24. Pu, R.; Ge, S.; Kelly, N.M.; Gong, P. Spectral absorption features as indicators of water status in coast live oak (*Quercus agrifolia*) leaves. *Int. J. Remote Sens.* **2003**, *24*, 1799–1810. [[CrossRef](#)]
25. Rollin, E.M.; Milton, E.J. Processing of high spectral resolution reflectance data for the retrieval of canopy water content information. *Remote Sens. Environ.* **1998**, *65*, 86–92. [[CrossRef](#)]
26. Zhang, C.; Pan, Z.; Dong, H.; He, F.; Hu, X. Remote Estimation of Leaf Water Content Using Spectral Index Derived from Hyperspectral Data. In Proceedings of the First International Conference on Information Science and Electronic Technology, ISET 2015, Wuhan, China, 21–22 March 2015; Volume 3, pp. 20–23.
27. Li, H.; Yang, W.; Lei, J.; She, J.; Zhou, X. Estimation of leaf water content from hyperspectral data of different plant species by using three new spectral absorption indices. *PLoS ONE* **2021**, *16*, e0249351. [[CrossRef](#)] [[PubMed](#)]
28. Riano, D.; Vaughan, P.; Chuvieco, E.; Zarco-Tejada, P.J.; Ustin, S.L. Estimation of fuel moisture content by inversion of radiative transfer models to simulate equivalent water thickness and dry matter content: Analysis at leaf and canopy level. *IEEE Trans. Geosci. Remote Sens.* **2005**, *43*, 819–826. [[CrossRef](#)]
29. Verhoef, W. Light scattering by leaf layers with application to canopy reflectance modeling: The SAIL model. *Remote Sens. Environ.* **1984**, *16*, 125–141. [[CrossRef](#)]
30. Xu, B.Q.; Guo, B.H.; Fan, S.H.; Su, W.H.; Zhao, J.C. Aboveground biomass allocation and nutrient dynamics of *Phyllostachys edulis* during the growth of young bamboo. *Chin. J. Trop. Crops* **2014**, *35*, 1481–1486.
31. Guo, C.F.; Guo, X.Y. Estimation of wetland plant leaf chlorophyll content based on continuum removal in the visible domain. *Acta Ecol. Sin.* **2016**, *36*, 6538–6546.
32. Mutanga, O.; Ismail, R. Variation in foliar water content and hyperspectral reflectance of *Pinus patula* trees infested by *Sirex noctilio*. *South. For.* **2010**, *72*, 1–7. [[CrossRef](#)]
33. Watt, M.S.; Leonardo, E.M.C.; Estarija, H.J.C.; Massam, P.; Silva, D.D.; O'Neill, R.; MacDougal, R.; Buddenbaum, H.; Zarco-Tejada, P.J. Long-term effects of water stress on hyperspectral remote sensing indicators in young radiata pine. *For. Ecol. Manag.* **2021**, *502*, 119707. [[CrossRef](#)]
34. Zarco-Tejada, P.J.; Miller, J.R.; Noland, T.L.; Mohammed, G.H.; Sampson, P.H. Scaling-up and model inversion methods with narrowband optical indices for chlorophyll content estimation in closed forest canopies with hyperspectral data. *IEEE Trans. Geosci. Remote Sens.* **2001**, *39*, 1491–1507. [[CrossRef](#)]
35. Gitelson, A.A.; Merzlyak, M.N. Remote estimation of chlorophyll content in higher plant leaves. *Int. J. Remote Sens.* **1997**, *18*, 2691–2697. [[CrossRef](#)]
36. Daughtry, C.S.T.; Walthall, C.L.; Kim, M.S.; de Colstoun, E.B.; McMurtrey, J.E., III. Estimating Corn Leaf Chlorophyll Concentration from Leaf and Canopy Reflectance. *Remote Sens. Environ.* **2000**, *74*, 229–239. [[CrossRef](#)]
37. Blackburn, G.A. Spectral indices for estimating photosynthetic pigment concentrations: A test using senescent tree leaves. *Int. J. Remote Sens.* **1998**, *19*, 657–675. [[CrossRef](#)]
38. Haboudane, D.; Miller, J.R.; Tremblay, N.; Zarco-Tejada, P.J.; Dextraze, L. Integrated narrow-band vegetation indices for prediction of crop chlorophyll content for application to precision agriculture. *Remote Sens. Environ.* **2002**, *81*, 416–426. [[CrossRef](#)]

39. Vogelmann, J.E.; Rock, B.N.; Moss, D.M. Red edge spectral measurements from sugar maple leaves. *Remote Sens.* **1993**, *14*, 1563–1575. [\[CrossRef\]](#)
40. Rouse, J.W.; Haas, R.H.; Schell, J.A.; Deering, D.W. Monitoring vegetation systems in the Great Plains with ERTS. *NASA Spec. Publ.* **1974**, *351*, 309.
41. Rondeaux, G.; Steven, M.; Baret, F. Optimization of soil-adjusted vegetation indices. *Remote Sens. Environ.* **1996**, *55*, 95–107. [\[CrossRef\]](#)
42. Roujean, J.L.; Breon, F.M. Estimating PAR absorbed by vegetation from bidirectional reflectance measurements. *Remote Sens. Environ.* **1995**, *51*, 375–384. [\[CrossRef\]](#)
43. Gamon, J.A.; Peñuelas, J.; Field, C.B. A narrow-waveband spectral index that tracks diurnal changes in photosynthetic efficiency. *Remote Sens. Environ.* **1992**, *41*, 35–44. [\[CrossRef\]](#)
44. Maire, G.L.; François, C.; Dufrêne, E. Towards universal broad leaf chlorophyll indices using PROSPECT simulated database and hyperspectral reflectance measurements. *Remote Sens. Environ.* **2004**, *89*, 1–28. [\[CrossRef\]](#)
45. Strachan, I.B.; Pattey, E.; Boisvert, J.B. Impact of nitrogen and environmental conditions on corn as detected by hyperspectral reflectance. *Remote Sens. Environ.* **2002**, *80*, 213–224. [\[CrossRef\]](#)
46. Ceccato, P.; Gobron, N.; Flasse, S.; Pinty, B.; Tarantola, S. Designing a spectral index to estimate vegetation water content from remote sensing data: Part 1: Theoretical approach. *Remote Sens. Environ.* **2002**, *82*, 188–197. [\[CrossRef\]](#)
47. Seelig, H.D.; Hoehn, A.; Stodieck, L.S.; Klaus, D.M.; Adams, W.W., III; Emery, W.J. The assessment of leaf water content using leaf reflectance ratios in the visible, near-, and short-wave-infrared. *Int. J. Remote Sens.* **2008**, *29*, 3701–3713. [\[CrossRef\]](#)
48. Huntjr, E.; Rock, B. Detection of changes in leaf water content using near-and middle-infrared reflectances. *Remote Sens. Environ.* **1989**, *30*, 43–54. [\[CrossRef\]](#)
49. Rock, B.N.; Vogelmann, J.E.; Williams, D.L.; Vogelmann, A.F.; Hoshizaki, T. Remote detection of forest damage. *Bioscience* **1986**, *36*, 439–445. [\[CrossRef\]](#)
50. Hardisky, M.A.; Klemas, V.; Smart, M. The influence of soil salinity, growth form, and leaf moisture on the spectral radiance of *Spartina alterniflora* canopies. *Photogramm. Eng. Remote Sens.* **1983**, *49*, 77–83.
51. Gao, B.C. NDWI—A normalized difference water index for remote sensing of vegetation liquid water from space. *Remote Sens. Environ.* **1996**, *58*, 257–266. [\[CrossRef\]](#)
52. Rodríguez-Pérez, J.R.; Riaño, D.; Carlisle, E.; Ustin, S.; Smart, D.R. Evaluation of hyperspectral reflectance indexes to detect grapevine water status in vineyards. *Am. J. Enol. Vitic.* **2007**, *58*, 302–317. [\[CrossRef\]](#)
53. Chen, D.; Huang, J.; Jackson, T.J. Vegetation water content estimation for corn and soybeans using spectral indices derived from MODIS near-and short-wave infrared bands. *Remote Sens. Environ.* **2005**, *98*, 225–236. [\[CrossRef\]](#)
54. Gao, B.C.; Heidebrecht, K.B.; Goetz, A.F.H. Derivation of scaled surface reflectances from AVIRIS data. *Remote Sens. Environ.* **1993**, *44*, 165–178. [\[CrossRef\]](#)
55. Fensholt, R.; Sandholt, I. Derivation of a shortwave infrared water stress index from MODIS near-and shortwave infrared data in a semiarid environment. *Remote Sens. Environ.* **2003**, *87*, 111–121. [\[CrossRef\]](#)
56. Zarco-Tejada, P.J.; Ustin, S.L. Modeling canopy water content for carbon estimates from MODIS data at land EOS validation sites. In Proceedings of the IEEE 2001 International Geoscience and Remote Sensing Symposium, Sydney, Australia, 9–13 July 2001; pp. 342–344.
57. Elvidge, C.D.; Lyon, R.J.P. Estimation of the vegetation contribution to the 1.65/2.22 μm ratio in airborne thematic-mapper imagery of the Virginia Range, Nevada. *Int. J. Remote Sens.* **1985**, *6*, 75–88. [\[CrossRef\]](#)
58. Peuelas, J.; Filella, I.; Biel, C.; Serrano, L.; Sav, R. The reflectance at the 950–970 nm region as an indicator of plant water status. *Int. J. Remote Sens.* **2007**, *14*, 1887–1905. [\[CrossRef\]](#)
59. Penuelas, J.; Pinol, J.; Ogaya, R.; Filella, I. Estimation of plant water concentration by the reflectance water index WI (R900/R970). *Int. J. Remote Sens.* **1997**, *18*, 2869–2875. [\[CrossRef\]](#)
60. Butler, W.L.; Hopkins, D.W. Higher derivative analysis of complex absorption spectra. *Photochem. Photobiol.* **2010**, *12*, 439–450. [\[CrossRef\]](#)
61. Kumar, L. High-spectral resolution data for determining leaf water content in *Eucalyptus* species: Leaf level experiments. *Geocarto Int.* **2007**, *22*, 3–16. [\[CrossRef\]](#)
62. Zhao, L.Y.; Deng, X.P.; Shan, L. A review on types and mechanisms of compenstion effect of crops under water deficit. *Chin. J. Appl. Ecol.* **2004**, *15*, 523–526.
63. Yu, L.; Cai, H.; Zhao, D. Prediction of length-of-day variation using grey relational analysis and extreme learning machine. *J. Univ. Chin. Acad. Sci.* **2015**, *32*, 588–593.
64. Tao, L.H.; Xu, J.L.; Feng, H.K.; Yang, G.J.; Yang, X.D.; Niu, Y.C. Winter Wheat Yield Estimation Based on UAV Hyperspectral Remote Sensing Data. *Trans. Chin. Soc. Agric. Mach.* **2020**, *51*, 146–155.
65. Huang, X.Y.; Xu, Z.H.; Yang, X.; Shi, J.M.; Hu, X.Y.; Ju, W.M. Monitoring the severity of *Pantana phyllostachysae* chao on bamboo using leaf hyperspectral data. *Remote Sens.* **2021**, *13*, 4146. [\[CrossRef\]](#)
66. Li, L.W.; Li, N.; Zang, Z.; Lu, D.S.; Wang, G.X.; Wang, N. Examining phenological variation of on-year and off-year bamboo forests based on the vegetation and environment monitoring on a New Micro-Satellite (VEN μ S) time-series data. *Int. J. Remote Sens.* **2020**, *42*, 2203–2219. [\[CrossRef\]](#)
67. Tibshirani, R.J. Regression Shrinkage and Selection via the LASSO. *J. R. Stat. Soc. Ser. B Methodol.* **1996**, *73*, 273–282. [\[CrossRef\]](#)

68. Hsiao, T.C. Plant responses to water stress. *Annu. Rev. Plant Physiol.* **1973**, *24*, 519–570. [[CrossRef](#)]
69. Donovan, S.D.; MacLean, D.A.; Zhang, Y.; Lavigne, M.B.; Kershaw, J.A. Evaluating annual spruce budworm defoliation using change detection of vegetation indices calculated from satellite hyperspectral imagery. *Remote Sens. Environ.* **2021**, *253*, 112204. [[CrossRef](#)]
70. Li, K.; Chen, Y.Z.; Xu, Z.H.; Huang, X.Y.; Hu, X.Y.; Wang, X.Q. Hyperspectral Estimation Method of Chlorophyll Content in MOSO Bamboo under Pests Stress. *Spectrosc. Spectr. Anal.* **2020**, *40*, 2578–2583.
71. Liu, Y.; Zhan, Z.; Ren, L.; Ze, S.; Yu, L.; Jiang, Q.; Luo, Y. Hyperspectral evidence of early-stage pine shoot beetle attack in Yunnan pine. *For. Ecol. Manag.* **2021**, *497*, 119505. [[CrossRef](#)]
72. Nabity, P.D.; Hillstrom, M.L.; Lindroth, R.L.; DeLucia, E.H. Elevated CO₂ interacts with herbivory to alter chlorophyll fluorescence and leaf temperature in *Betula papyrifera* and *Populus tremuloides*. *Oecologia* **2012**, *169*, 905–913. [[CrossRef](#)]
73. Fu, H.Y. Study on Remote Sensing Estimation Model of Main Biochemical Parameters of Tobacco Leaver Based on Non-Imaging Hyperspectral. Master's Thesis, Southwest Forestry University, Kunming, China, 2015.
74. Chu, X.P. Classification Research Based on Non-Imaging Hyperspectral Data. Master's Thesis, Zhejiang A&F University, Hangzhou, China, 2012.

Disclaimer/Publisher's Note: The statements, opinions and data contained in all publications are solely those of the individual author(s) and contributor(s) and not of MDPI and/or the editor(s). MDPI and/or the editor(s) disclaim responsibility for any injury to people or property resulting from any ideas, methods, instructions or products referred to in the content.